

An Optical Catalog of Galaxy Clusters Obtained from an Adaptive Matched Filter Finder Applied to SDSS DR6

T. Szabo¹, E. Pierpaoli¹, F. Dong², A. Pipino^{1,3,4}, J. Gunn²

tszabo@usc.edu, pierpaol@usc.edu

ABSTRACT

We present a new cluster catalog extracted from the Sloan Digital Sky Survey Data Release 6 (SDSS DR6) using an adaptive matched filter (AMF) cluster finder. We identify 69,173 galaxy clusters in the redshift range $0.045 \leq z < 0.78$ in 8420 sq. deg. of the sky. We provide angular position, redshift, richness, core and virial radii estimates for these clusters, as well as an error analysis for each of these quantities. We also provide a catalog of more than 205,000 galaxies representing the three brightest galaxies in the r band which are possible BCG candidates. We show basic properties of the BCG candidates and study how their luminosity scales in redshift and cluster richness. We compare our catalog with the maxBCG and GMBCG catalogs, as well as with that of Wen, Han, and Liu. We match between 30% and 50% of clusters between catalogs over all overlapping redshift ranges. We find that the percentage of matches increases with the richness for all catalogs. We cross match the AMF catalog with available X-ray data in the same area of the sky and find 539 matches, 119 of which with temperature measurements. We present scaling relations between optical and X-ray properties and cluster center comparison. We find that both Λ_{200} and R_{200} correlate well with both L_X and T_X , with no significant difference in trend if we restrict the matches to flux-limited X-ray samples.

Subject headings: galaxies: clusters: general — galaxies: distances and redshifts

1. Introduction

Galaxy clusters are the most massive gravitationally bound systems in the Universe. Their study has been pursued for many different astrophysical and cosmological reasons: their mass function allows for the determination of the several cosmological parameters, including the mass density,

¹Department of Physics and Astronomy, University of Southern California, Los Angeles, CA 90089, USA

²Department of Astrophysical Sciences, Princeton University, Princeton, NJ 08544, USA

³Dipartimento di Fisica, sez. Astronomia, Università di Trieste, via G.B. Tiepolo 11, I-34131, Trieste, Italy

⁴Department of Physics and Astronomy, University of California at Los Angeles, Los Angeles, CA 90095, USA

Ω_m , and the matter power spectrum normalization σ_8 (Pierpaoli, et al. 2001; Reiprich & Böhringer 2002; Seljak 2002; Pierpaoli, et al. 2003; Dahle 2006; Pedersen & Dahle 2007; Rines et. al. 2007; Rozo et al. 2009) as well as the dark energy equation of state (Allen et al. 2008) and neutrino masses (Wang et al. 2005). Furthermore, cluster surveys allow the determination of their clustering properties inferring information on the large scale structure (Bahcall 1988; Postman et al. 1992; Carlberg et al. 1996; Bahcall et al. 1997). Due to their high galaxy density, clusters are excellent laboratories for studying galaxy evolution (Dressler 1980; Butcher & Oemler 1978; Garilli et al. 1999; Goto et al. 2003a,b). Clusters can also be used as gravitational lenses, providing a way to constrain their masses, as well as to study distant galaxies (Blain et al. 1999; Smail et al. 2002; Metcalfe et al. 2003; Santos et al. 2004). More recently, cluster abundances and internal structure have been invoked as test for modified gravity (Rapetti et al. 2008; Diaferio & Ostorero 2009).

Clusters are observed in several bands: in the optical through the overdensity of galaxies or their color properties, and in the radio and X-ray through the emission of the intra-cluster medium. While optical observations were the first ones to be performed, X-ray surveys of the past twenty years have discovered hundreds of clusters up to high redshifts ($z \simeq 1$), while radio surveys aiming at detecting galaxy clusters through their Sunyaev–Zel’dovich (SZ) effect are underway. This plethora of data reinvigorates the interest in galaxy clusters as it will provide a better understanding of cluster physics and the selection function for each detection method, therefore improving the precision in deriving cosmological constraints.

In this paper, we focus on optical observations of clusters in the Sloan Digital Sky Survey (SDSS), presenting the cluster catalog constructed from an adaptive match filter (AMF) technique (Dong et al. 2008; Postman et al. 1996; Kepner et al. 1999; Kim et al. 2002; White & Kochanek 2002).

SDSS provides luminosities in five bands and redshift estimates for millions of galaxies in more than one-fifth of the sky. This has allowed automated algorithms to compile catalogs of clusters objectively by identifying overdensities in galaxy distributions. Three such optical cluster catalogs include the maxBCG catalog (Koester et al. 2007) constructed from SDSS DR5, another catalog from SDSS DR6 constructed by Wen et al. (2009, hereafter, WHL), and the Gaussian Mixture Brightest Cluster Galaxy catalog (Hao et al. 2010, hereafter, GMBCG) which is based on SDSS DR7. The maxBCG catalog makes use of a ridgeline in $g-r$ magnitudes to determine photometric redshifts and cluster membership. The catalog by WHL uses a friends-of-friends algorithm to associate galaxies above a specific luminosity cut. The GMBCG catalog is a follow-up to the maxBCG catalog that extends the redshift range to $z = 0.55$ and uses statistics gathered from the maxBCG catalog to refine the cluster finding procedure. Given the diverse nature of clusters, one should not expect to detect the same object when different methods are applied to the same data. Comparisons between methods allow for a better understanding of selection biases of each method.

We present here the catalog extracted from the SDSS DR6 by applying the AMF technique tailored to handle SDSS data (Dong et al. 2008, hereafter, D08) and provide a comparison with

the maxBCG and GMBCG samples. We also compare our catalog with the WHL catalog, which was also derived from DR6 data. While our finder also uses overdensities as a starting point for determining the presence of a cluster, it does not make *a priori* assumptions about the color or number of bright galaxies. This approach potentially allows for the detection of clusters which do not have a bright red galaxy. Moreover, our finder only relies on extremizing a likelihood function, which provides a very general method for characterizing cluster properties such as their size, richness and core radius during their detection.

Clusters may also be detected in the X-ray band, which traces their diffuse gas component. Both X-ray and optical observations are used to determine cluster masses and derive cosmology. However, these two bands trace different physical components of the cluster, so they represent quite different probes of the state of the cluster. Selection effects for optical and X-ray are different, and each method for estimating masses may have intrinsic biases and limitations. Now that big optical cluster samples are available, it is possible to assess to what extent optical and X-ray properties are related and probe the reliability of various methods for mass estimate and cosmology derivation. In addition, galaxy clusters have now been detected via their SZ effect (Staniszewski et al. 2009). Comparisons between the optical properties and the SZ effect (Pipino and Pierpaoli 2010) using the Planck Early Release Compact Source Catalog (Planck Collaboration 2011) will be the subject of a future paper.

As a first step in this direction, various authors have measured scaling relations between X-ray observables such as luminosity (L_X) and temperature (T_X) and optical richness (Lopes et al. 2006; Rykoff et al. 2008; Popesso et al. 2005; Koester et al. 2007). While the richness measure used didn't seem to correlate well with X-ray luminosity, the lensing-derived mass for richness bin showed a remarkable correlation with L_X . These results were based on shallower and smaller optical cluster samples than the one presented here as they only relied on a sample on the order of 100 matches. Here we provide the X-ray matches for our AMF cluster sample with all available X-ray cluster data from the BAX database and with the flux limited NORAS samples (Böhringer et al. 2000, 2004). We also measure scaling relations between optical richness and X-ray properties for matching clusters. We find good correlation between optical richness and both X-ray luminosity and temperature.

A feature of galaxy clusters that is often considered for its own study is the brightest cluster galaxy (BCG). As part of this work, we determined the three brightest galaxies in any cluster in the r -band and include a list of them as potential BCGs. These can be used as a further basis for comparison between our clusters and those in the maxBCG and other catalogs. Moreover, BCGs can be exploited as tracers of large scale structure in cross correlation analysis with other catalogs (Ho et al. 2009). A detailed study of a sub-sample of BCGs selected to be the brightest and to have $z \leq 0.3$ in terms of colors and X-ray and UV counterparts is presented in a companion paper (Pipino et al. 2010).

The organization of this paper is as follows. In section 2, we discuss the specifics of the SDSS

data used. We present the AMF cluster finder and details on its application to the SDSS data in section 3. Section 4 discusses the characterization of the galaxy cluster catalog and of the related BCGs sample. In section 5 we compare our catalog with the maxBCG, WHL, and GMBCG ones, as well as with X-ray cluster catalogs. Section 6 is dedicated to the conclusions.

Unless stated otherwise, we assume a Λ CDM cosmology, with $\Omega_m = 0.3$ and $\Omega_\Lambda = 0.7$, and $H_0 = 100 \text{ h km s}^{-1} \text{ Mpc}^{-1}$.

2. SDSS Data

The Sloan Digital Sky Survey (York et al. 2000; Adelman-McCarthy, et al. 2008) is a five-band CCD imaging survey of 10^4 deg^2 in the high latitude North Galactic Cap and a smaller deeper region in the South, followed by an extensive multi-fiber spectroscopic survey. The imaging survey is carried out in drift-scan mode in five SDSS filters (u, g, r, i, z) to a limiting magnitude of $r < 22.6$ for 50% completeness (Adelman-McCarthy, et al. 2007). The spectroscopic survey targets 8×10^5 galaxies to approximately $r < 17.7$, with a median redshift of $z = 0.1$, and a smaller deeper sample of 10^5 Luminous Red Galaxies (LRGs) out to about $z = 0.5$. In this paper we construct a cluster catalog for Data Release 6 (DR6)¹ and chose to use the photometric redshifts provided by Oyaizu et al. (2008). In total, we have redshift information for $> 98\%$ of 67.6 million galaxies that covered $\sim 8,420 \text{ deg}^2$ in stripes 9-39, 42-44, 76, 82 and 86. In this sample, there are 7.4×10^5 with spectra. The median error for photometric redshift (z_{photo}) measurements is 0.12. All galaxy measurements were extracted from the **Galaxy** view on the CasJobs DR6 database using the **FLAGS** as described in Appendix A to limit our sample to galaxies with good photometry. We use the **cc2** photo-z estimates in order to avoid a possible bias from applying the luminosity function twice, once in the choice of photometric redshifts and again as part of the AMF likelihood calculation.

It is important to understand the errors in photometric redshifts when using our technique, as we explain below. We used the photometric redshifts provided by Oyaizu et al. (2008) in preference to those from Csabai et al. (2003), even though the latter were available for the whole of DR6, because the errors on z_{photo} for Csabai et al. (2003) were underestimated. The Oyaizu *et al* errors on z_{photo} are much closer to the errors $|z_{spec} - z_{photo}|$ estimated from the sub-sample of galaxies which have spectroscopic redshifts. The Csabai et al. (2003) estimates would bias our redshift filter in such a way that would eliminate galaxies that should be considered as possibly belonging to a given cluster. The width of the filter is determined by the error estimate in redshift. Also, the Oyaizu et al. (2008) sample is truncated at an r -band magnitude of 22. This is important, as the behavior of the luminosity function that we use is not well-understood above this magnitude. In addition, the coverage for the region of the sky over which we are constructing our catalog is much more uniform for the redshifts provided by Oyaizu et al. (2008) than for those provided by

¹<http://cas.sdss.org/dr6>

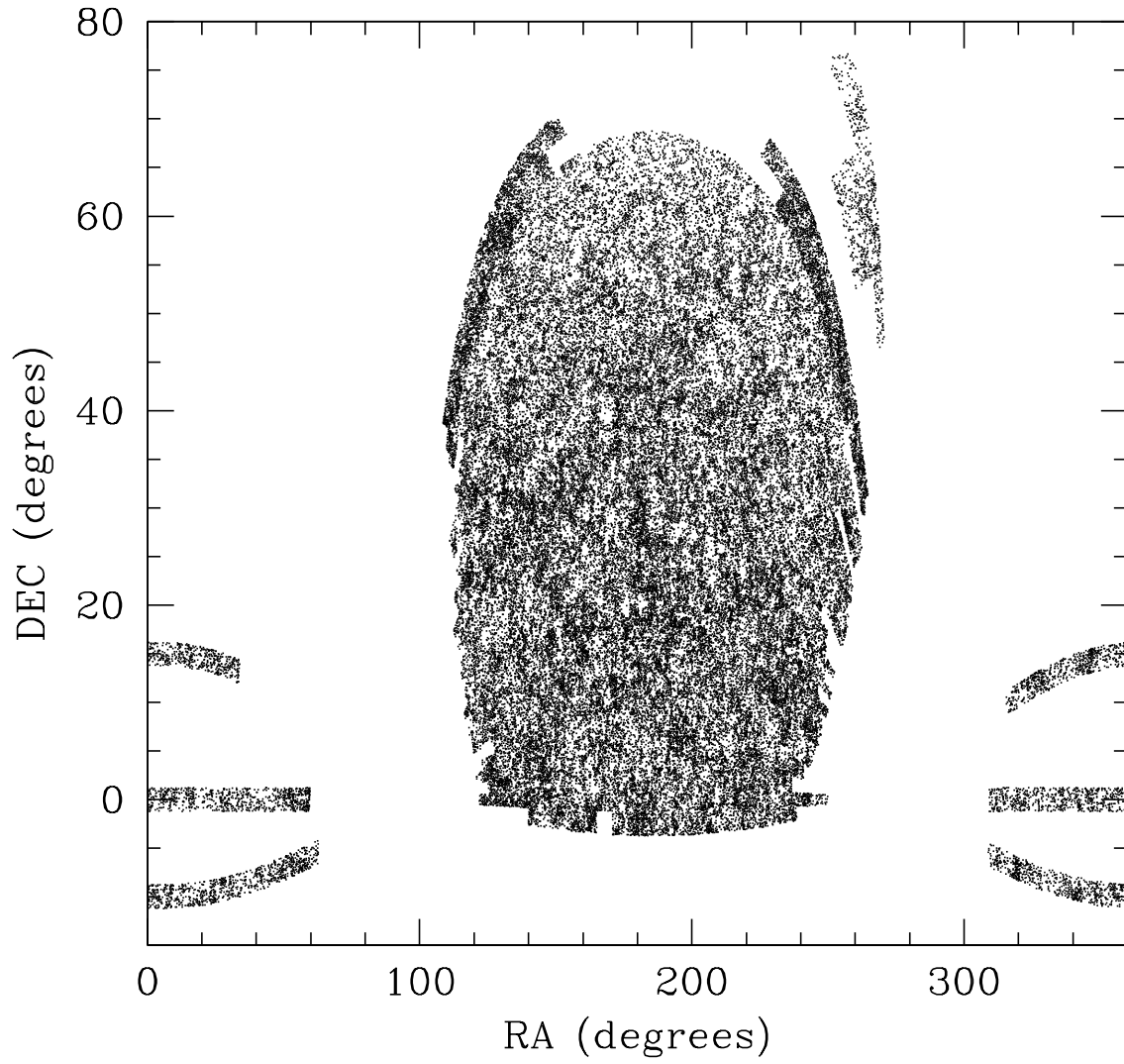


Fig. 1.— Angular positions of the clusters found in SDSS DR6.

Csabai et al. (2003) for SDSS DR6. Simulations using a mock galaxy catalog indicated that this procedure should lead to a catalog that is >90% complete at least to $z = 0.4$ (D08).

The current catalog is constructed using r -band data information only, although the code could be extended to make use of information in all bands. Figure 1 shows the distribution of clusters in our catalog on the sky. We will assess data based on the continuity and completeness of its redshift estimates for future releases of AMF cluster catalogs.

3. The Cluster Finder

3.1. Method

The cluster finder that we employ is based on the matched filter concept (Postman et al. 1996; Kawasaki et al. 1998; Kepner et al. 1999; Kim et al. 2002; White & Kochanek 2002). A complete description of the method used here as well as results of testing on mock data is available in D08.

The matched filter technique adopted here is a likelihood method which identifies clusters by convolving the optical galaxy survey with a set of filters based on a modeling of the cluster and field galaxy distributions. A cluster radial surface density profile, a galaxy luminosity function, and redshift information (either photometric or spectroscopic when available) are used to construct filters in position, magnitude, and redshift space, from which a cluster likelihood map is generated. The peaks in the map thus correspond to candidate cluster centers where the matches between the survey data and the cluster filters are optimized. The algorithm automatically provides the probability for the detection, best-fit estimates of cluster properties including redshift, radius and richness, as well as a framework for membership assessment for each galaxy.

The cluster finding algorithm computes the likelihood on a grid whose points are centered on the positions of galaxies. The finder uses an iterative procedure that determines which galaxy maximizes the difference in likelihood from the previous step that a cluster exists that is centered on that galaxy. This cluster is then added to the list of identified clusters, and the procedure continues with the remaining galaxies. The parameters of the new cluster (redshift z_c , core radius r_c and richness Λ_{200}) are varied in order to maximize its likelihood increment. The radius R_{200} of the cluster is determined by computing at which distance from the central galaxy the overdensity of galaxies is 200 times the critical density, assuming the average galaxy density is representative of the mean mass density. The richness is the total luminosity within R_{200} in terms of L^* , where L^* evolves passively as a function of redshift, brightening by 0.8 mag from $z = 0$ to $z = 0.5$ (Loveday et al. 1992; Lilly et al. 1995; Nagamine et al. 2001; Blanton et al. 2003; Loveday 2004; Baldry et al. 2005; Ilbert et al. 2005). We assume that L^* does not vary with the cluster richness, but see Hansen et al. (2009) and section 4.3. The cluster finding procedure is stopped when the natural logarithm of the likelihood for any new cluster is below zero. (For the remainder of this paper, any mention of a value of the likelihood refers to the $\ln(\text{likelihood})$.) From this sample of

cluster candidates, all clusters with richness ≥ 10 are chosen for recentering, which is described below.

Since the matched filter technique does not explicitly use the information about the red sequence to select clusters as in some color-based cluster-finding methods (Annis et al. 2002; Miller et al. 2005; Koester et al. 2007), it can theoretically detect clusters of any type in color, and is not restricted only to old, red E/S0 galaxies. Such clusters likely dominate the cluster population, but may not constitute all of it especially as one probes systems of lower richness and at higher redshifts. We refer the reader to Pipino et al. (2010) for further discussion on this issue.

3.2. Completeness and Purity Estimate

By applying this cluster finder to simulations, D08 demonstrated that, with a richness cut at $\Lambda_{200} \geq 20$, the results of this finder are over 95% complete for objects with $M_{200} > 2.0 \times 10^{14} h^{-1} M_{\odot}$ and $\sim 85\%$ complete for objects with $M_{200} > 1.0 \times 10^{14} h^{-1} M_{\odot}$ in the redshift range $0.10 < z < 0.45$. These authors also showed that the finder produces a catalog that is over 95% pure for clusters with $\Lambda_{200} > 30$ and 90% pure for clusters with $\Lambda_{200} > 20$ over all redshifts $z < 0.45$. No testing has been performed on deeper simulations, so that we are not in the position of making statements of purity and completeness for any redshift beyond $z = 0.45$.

3.3. Recentering of Clusters

The initial run of the finder produces clusters that are centered on observed galaxies. However, there is no reason to assume that the actual center of mass for the cluster should necessarily be located on a galaxy.

In general, finding the correct center of mass of a cluster is important for several reasons: *i*) for mass estimation with the lensing effect, as clusters are stacked one on top of the other; *ii*) for comparison with measurement of the cluster in other bands, *iii*) for assessing velocity dispersions and therefore kinetic mass estimates of the cluster; *iv*) for the purpose of cross-correlations with other surveys and CMB maps. Moreover, trying to determine cluster’s properties that rely on a spherical model while not using the correct center may lead to determining them poorly and assigning a bigger error to them.

For all these reasons, after the clusters have been identified, it is necessary to relax the hypothesis that clusters are centered on a galaxy and refine the center position as well as the characterizations of the clusters. We therefore recompute the cluster’s likelihood for each cluster in the sample by varying the new hypothetical center on a fine grid of resolution $1 \text{ h}^{-1} \text{ kpc}$ and whose extent is the core radius, r_c . About 37% of the clusters have their center shifted by at least $1 \text{ h}^{-1} \text{ kpc}$; the average displacement for clusters whose center is measurably displaced is $65^{+32}_{-58} \text{ h}^{-1} \text{ kpc}$.

All other quantities (Λ_{200} , R_{200} , z , and r_c) are recomputed for the new angular position.

3.4. Blended clusters

The procedure outlined above finds 69,173 clusters with $\Lambda_{200} \geq 20$ in DR6. These clusters are distributed over 66,231 unique sites in angular and redshift space. To determine unique sites, we first determine which galaxies have a high likelihood of belonging to each cluster. We then determine the three brightest galaxies in the r -band for each cluster. Clusters which share any of the three brightest members are said to belong to the same site. The cluster with the highest likelihood at a given site is said to be the primary cluster. Since the richness scales as the likelihood, this is also the richest cluster at a site.

To assign galaxies to a particular cluster, we make a list of all galaxies (i) that may belong to a cluster (k) such that the angular displacement of the galaxy from a cluster center is less than $R_{200,k}/d_A(z_i, \Omega_m, \Omega_\Lambda)$ and $|z_k - z_i| < 3\sigma_z(i)$. Here, $\sigma_z(i)$ is the estimate of the error in photometric redshift assigned to the galaxy in SDSS DR6 and d_A is the angular diameter distance to the galaxy, i . This is not a final membership list for the set of clusters, but a set of galaxies that could contribute, however minimally, to the likelihood and richness of a cluster. For galaxies within R_{200} of the center of the cluster, we then find the likelihood of the cluster when it is missing galaxy i . The difference between the likelihood of the cluster with all members included and the likelihood when missing galaxy i is referred to as the likelihood difference, \mathcal{L}_i . We then assign memberships of galaxies to a cluster by selecting galaxies that lie within R_{200} from the cluster’s center, and have at least $\mathcal{L}_i = 1$. With this threshold, we can assign member galaxies to >99.4% of the clusters. This cutoff preserves galaxies with a spectroscopic redshift measurement that is close to the redshift of the cluster as cluster members. Selecting a cutoff of $\mathcal{L}_i > 1$ quickly reduces the percentage of clusters with members assigned, and a cutoff < 1 includes too many bright galaxies with no redshift estimate. This choice of cutoff also reduces the median value of the error in photometric redshift for galaxies chosen to be cluster members to 0.062. We do not apply a prescribed redshift cut because the high likelihood cut applied already ensures that the selected galaxies are close to the cluster’s center. The galaxies selected with this criterion are included in the catalog (see Table B.4).

By using this method to determine the brightest galaxies in a cluster and requiring that the brightest galaxies can only belong to one site, we determine that <5% of sites have more than one cluster attributed to them. We choose to retain these blended clusters in the catalog as possible subjects of cluster mergers. We also want to know how these sites compare with detections in other bands. Lastly, these blended clusters provide insight into the AMF filter detection method.

4. The AMF Catalog

In this section we present the AMF cluster catalog and the associated BCG. We present its main properties including richness, redshift distribution, core radius with associated errors. We describe how the BCG catalog is assembled and present its main properties in the r band. A description on how the data are released and how to retrieve them is in the Appendix.

4.1. Main Properties

The catalog contains 69,173 clusters with $\Lambda_{200} \geq 20$ over an area of $\sim 8,420 \text{ deg}^2$. Results of the cluster finder applied to simulations (D08) associate this richness threshold with an approximate mass of $4 \times 10^{13} M_{\odot}$, according to:

$$\Lambda_{200} = (47.2 \pm 4.1) \times \left(\frac{M_{200}}{10^{14} h^{-1} M_{\odot}} \right)^{1.03 \pm 0.04} \quad (1)$$

Using this result from the simulation as a guideline, we detect that there are about 5000 clusters in our new AMF SDSS catalog with a mass above $10^{14} h^{-1} M_{\odot}$ (roughly corresponding to richness 50); 2700 of which are nearer than $z = 0.4$. It should be kept in mind, however, that eq.1 was derived on the basis of simulations where the galaxy colors were assigned to dark matter particles, so this result may not necessarily correspond precisely to what we observe in nature. The exponent in the relation is different from one only by statistical error, and merely reflects the mass-to-light ratio of cluster galaxies assumed in the simulations. A proper calibration of the mass–richness relation should be made by evaluating masses for this sample possibly with different methods. This issue will be properly addressed in a future paper.

The position of the clusters in the sky is represented in fig. 1. It is clearly not homogeneous, as photometric redshifts are not determined in a uniform way on the sky. The density of clusters varies from stripe to stripe, with an average number of clusters per deg^2 of 7.2. The distribution of cluster density per deg^2 varies between 5.4–6.0 (stripes 43–44, 76, 82, and 86), 6.0–7.2 (stripes 9–37) and > 9 (stripes 38–39). The smallest density belongs to stripe 42 which has 4.04 clusters per deg^2 , and the largest density is in stripe 38 at 9.37 clusters per deg^2 . We are confident that the variations in cluster density in stripes 9–37 are due to large-scale structure. More work is needed to understand the density variations in other stripes.

The distribution of our clusters in richness for different redshift bins is shown in fig. 2. As expected, the ratio of high richness objects over low richness ones decreases for increasing redshift. The richest clusters have richness values 168, 254, 270, 226, and 172 in subsequent redshift bins with $\Delta z = 0.1$ starting at $z = 0.1$. Note that the catalog is clearly not complete for $z > 0.5$. For this reason, the considerable drop in the number of very rich clusters compared to the low richness ones, although expected to a certain extent for structure formation reasons, may in fact be due to

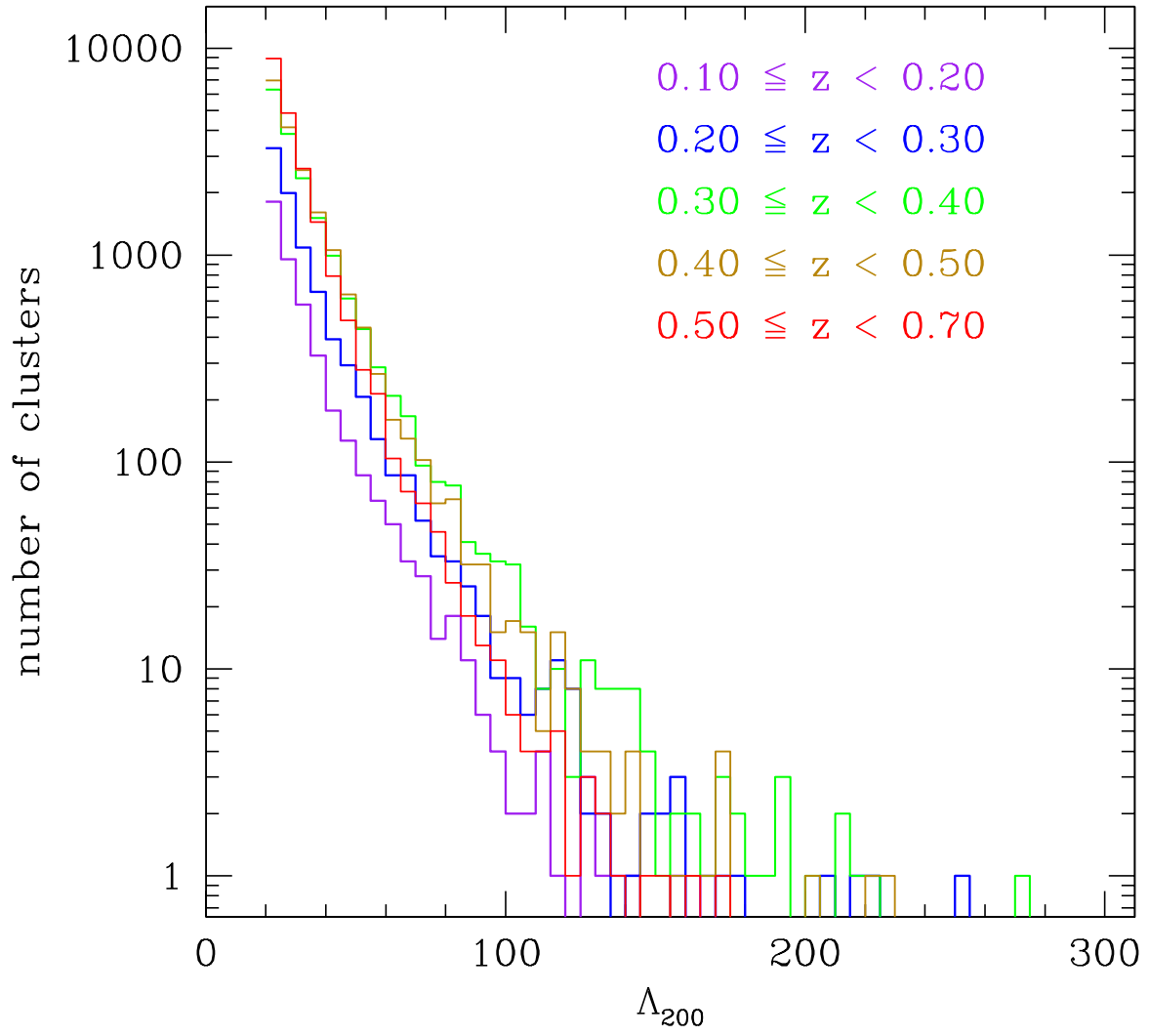


Fig. 2.— Distribution of AMF clusters in richness per redshift bin.

limitations of our searching method. A proper assessment of this issue would require comparison with other cluster finders performances at high redshifts or better understanding of this cluster finder on SDSS deeper data.

The redshift distribution of the cluster catalog is presented in fig. 3, together with the distribution of the maxBCG catalog. The green, dotted lines in this plot represents the number of clusters expected in each bin for $\sigma_8 = 0.8$ and 0.9 , and a mass threshold of $M = 4 \times 10^{13} h^{-1} M_\odot$, which corresponds to $\Lambda_{200} \sim 20$ according to eq. 1. The cluster sample redshift distribution has a peak at $z = 0.38$ and then roughly flattens until $z = 0.55$. However, clusters are found out to redshift 0.78 . The total number of clusters with redshift below $0.3, 0.4, 0.5, 0.78$ is, respectively: 13593, 30814, 49198, and 69173.

Histograms of the core radius and R_{200} are presented in fig. 4. The distribution in radii is fairly peaked around $0.8 h^{-1}$ Mpc, while the distribution of core radii is broader with some suggestion of bimodality. Most clusters have a core radius between 80 and $240 h^{-1}$ kpc.

Finally, we notice that the estimated radii correlate very well with richness (see fig. 5), as expected from tests on simulations (D08). The relationship between Λ_{200} and R_{200}^3 is linear, with a dispersion relation given by:

$$\sigma_{R_{200}} = (0.019 \pm 0.005)R_{200} + (0.026 \pm 0.006), \quad (2)$$

where $\sigma_{R_{200}}$ is measured in h^{-1} Mpc.

4.2. Error Determination

For each cluster found, the catalog reports the maximum likelihood value for the three main parameters (Λ_{200} , z , and r_c), as well as for the determination of R_{200} . The likelihood determination procedure also allows us to find the errors of the varied quantities (Λ_{200} , z , and r_c) as well as for the angular positions of clusters. In order to determine errors, the likelihood for each cluster has been recomputed on a finer grid and only considering galaxies within $2R_{200}$ and $3\sigma_z$ of the cluster center. This larger distribution in angular space allows us to vary the location of the center to determine confidence regions in angular space. Errors on each quantity were found by exploring the likelihood surface in two of the parameters (e.g., r_c and Λ_{200}) while keeping the others fixed. The boundaries of the 68%, 90%, 95%, etc. confidence regions are determined by looking for the extrema of the parameters which give a difference in likelihood from the maximum value.

Errors for each cluster are reported in the catalog, and include the extrema of the 68% and 95% confidence range for each quantity. Table 1 gives errors as a function of Λ_{200} , table 2 as a function of redshift, and table 3 as a function of core radius. In these tables, the interquartile range is provided for each error estimate.

Errors in Λ_{200} were measured as a function of Λ_{200} , z , and r_c . The error in richness increases

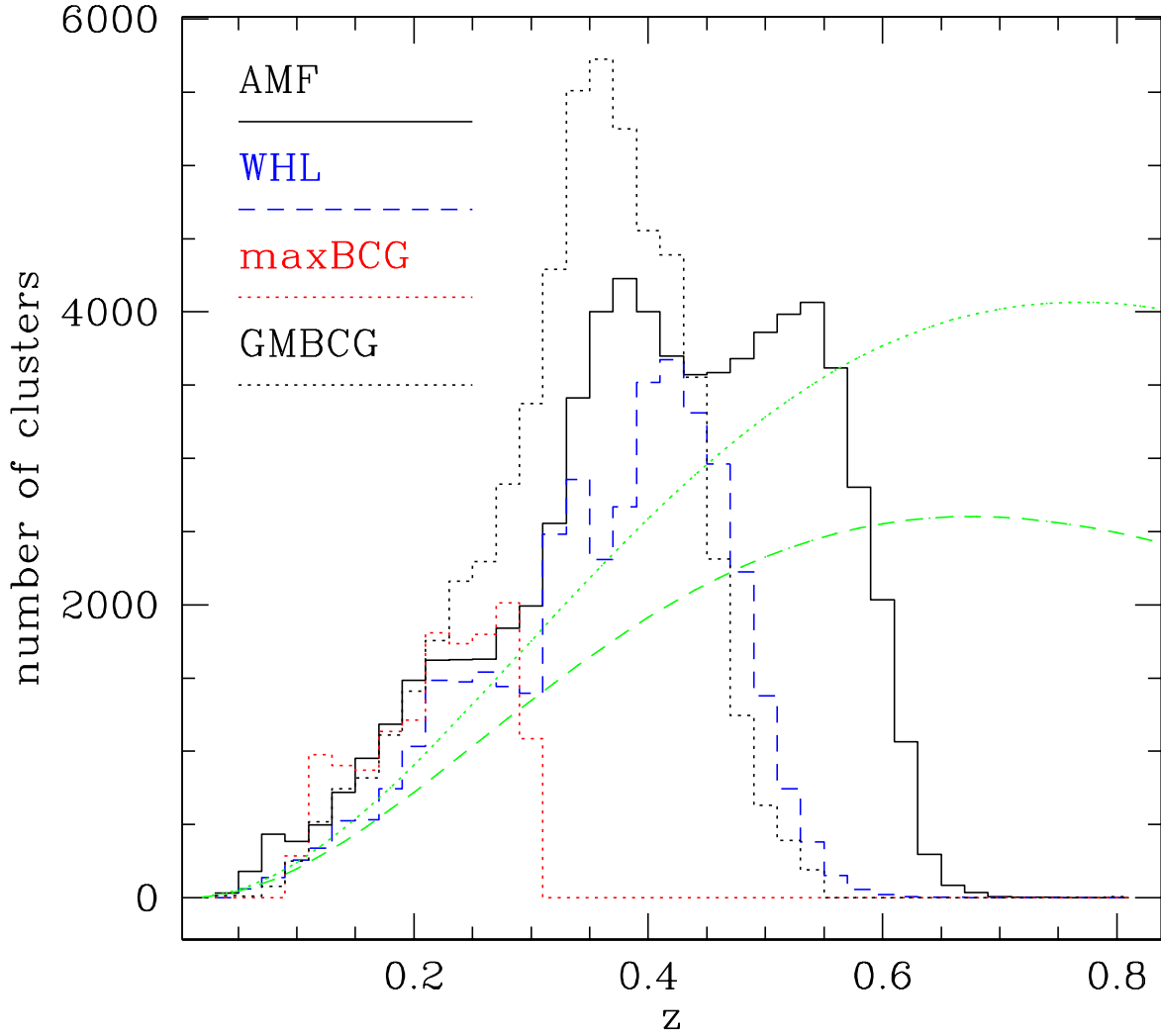


Fig. 3.— Redshift Distribution of AMF (solid line), WHL (dashed line, blue), maxBCG (dotted line, red), and GMBCG (dotted line, black) clusters. The green lines represent the expected number of clusters for $\sigma_8 = 0.8$ (dashed) and 0.9 (dotted) and a mass threshold of $4 \times 10^{13} h^{-1} M_\odot$. The value of $h = 0.70$. Note that the richness cutoff for the maxBCG and GMBCG catalogs is lower than that for the AMF catalog.

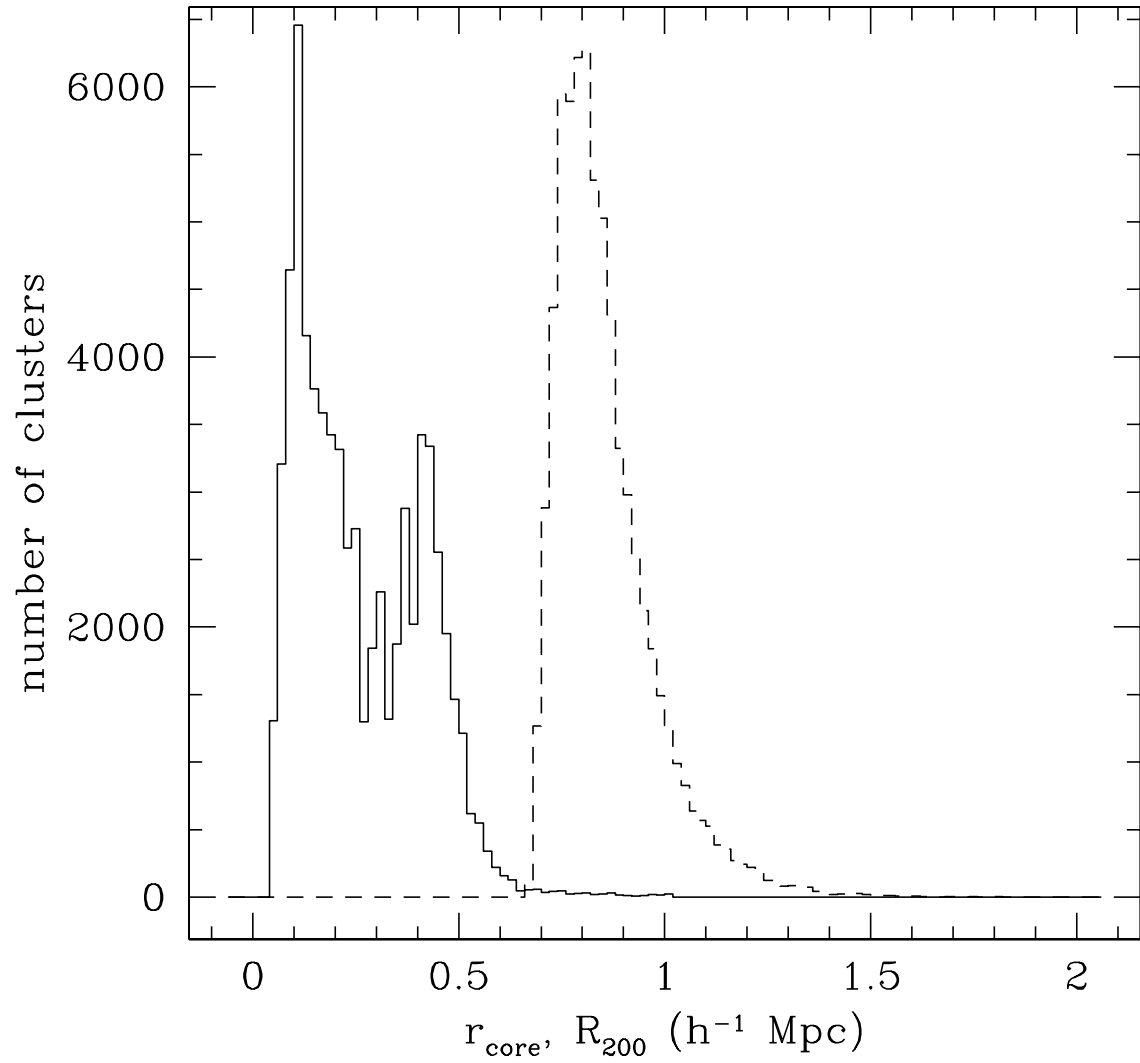


Fig. 4.— Distribution of AMF clusters as a function of core radius (solid line) and R_{200} (dashed line).

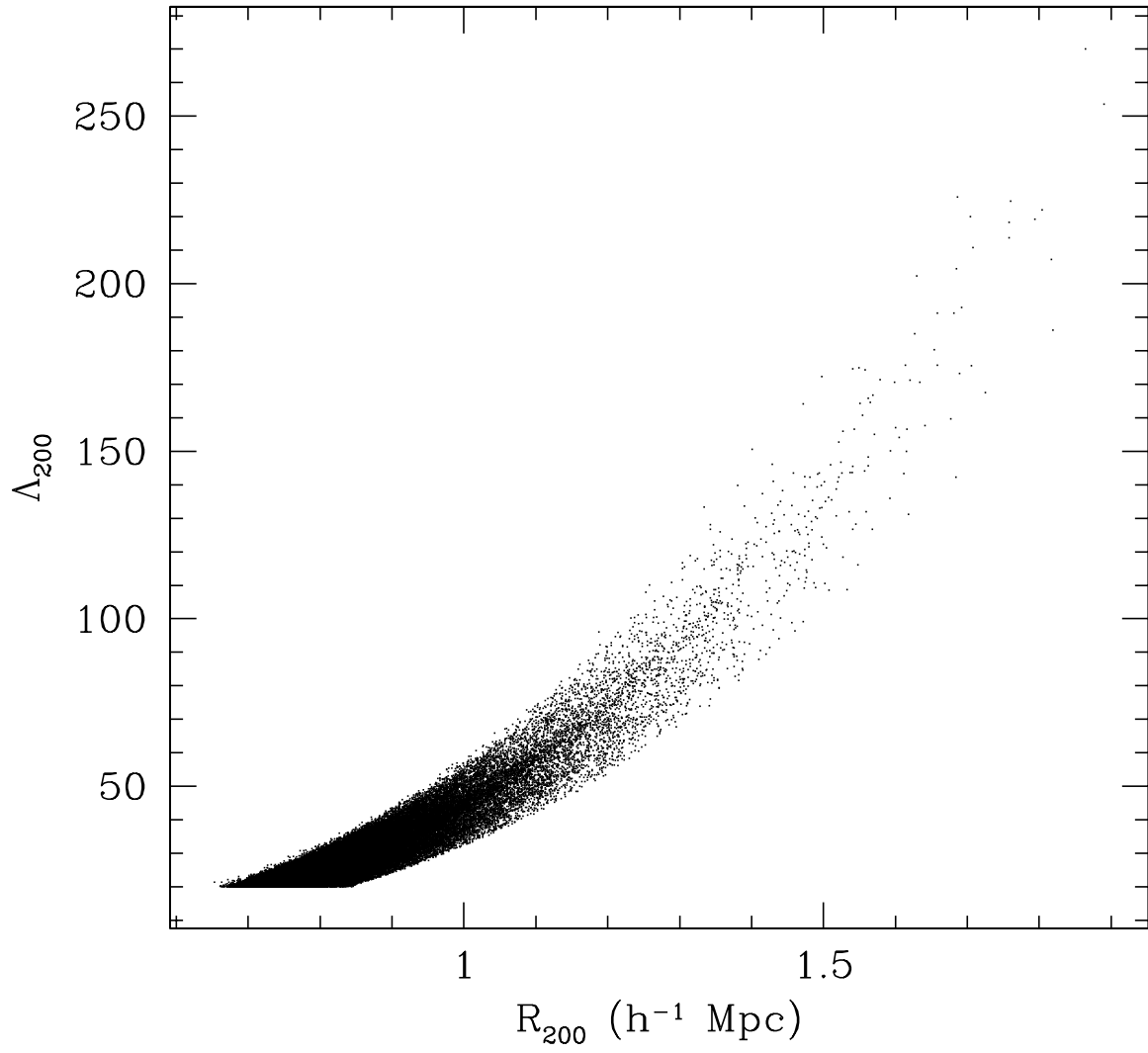


Fig. 5.— Plot of Λ_{200} vs. R_{200} for all 69,173 clusters.

as richness decreases. This is to be expected, as the addition or subtraction of one galaxy creates a larger percentage difference in smaller clusters. Typical values range from around 45% for clusters with $20 \leq \Lambda_{200} < 30$ to 15 to 20% for clusters with $\Lambda_{200} > 150$. Errors in Λ_{200} change very little as a function of z , though there is a small decrease with increasing redshift. Typical errors are $\sim 45\%$, as the smallest clusters are the ones that are most prevalent. The error in Λ_{200} is anti-correlated with the size of the core radius estimate. Clusters with core radii $< 0.1 \text{ h}^{-1} \text{ Mpc}$ have errors in Λ_{200} around 50%, and those with core radii $\geq 0.5 \text{ h}^{-1} \text{ Mpc}$ have richness errors typically in the vicinity of 37%. We also find that the average core radius grows steadily from $0.23 \text{ h}^{-1} \text{ Mpc}$ for clusters with $20 \leq \Lambda_{200} < 30$ to $0.43 \text{ h}^{-1} \text{ Mpc}$ for clusters with $\Lambda_{200} \geq 100$, so this anti-correlation is expected.

Several studies have indicated that the fit of an NFW profile for optical clusters tends to have a large error in core radius, r_c , and that in some cases, a function with either a core or a cusp in the density at the center of the cluster gives an adequate description (Katgert, Biviano, & Mazure 2004; Biviano & Salucci 2006). Our error analysis similarly finds the core radius to be poorly constrained in most cases. As with the other parameters, the error in core radius is smallest for the richest clusters, with errors falling between 14% and 36% for half of the 327 clusters with $\Lambda_{200} \geq 100$. For the 43,600 clusters with $20 \leq \Lambda_{200} < 30$, the endpoints of this range shift to 46% and 87%. The redshift of the cluster also has a strong effect on the typical error value for the core radius. Nearby clusters ($z \leq 0.2$) have errors that are about the same size as the estimate for the value of the core radius, while the errors drop to about half the core radius (40–70%) for clusters with $z \geq 0.4$. There is no clear trend in the error in core radius as a function of core radius, except that the values are greater than 40% for all clusters with $r_c < 0.5 \text{ Mpc h}^{-1}$.

As we discussed in section 3.3, our clusters are not required to be centered on a galaxy. This allows us to explore a generalized position in angular space to determine how accurately we found the cluster center. The errors are determined by varying the position of the center over the core radius of the cluster; therefore, it is important to note any dependence of error on r_c first. For $r_c \geq 0.2 \text{ h}^{-1} \text{ Mpc}$, the values of the boundaries for the middle 50% of the error values are consistently about 18% of R_{200} for the low end and about 32% for the high end. This is probably the best error estimate for clusters with $r_c < 0.2 \text{ h}^{-1} \text{ Mpc}$ as well, as it appears that varying the position over the core radius limits the maximum extent to which you can sample the likelihood surface for this set of clusters. Errors in angular position anti-correlate with the richnesses of the clusters. The richest clusters will have errors in position typically $< 10\%$ of R_{200} , while the poorest clusters in our catalog have position errors usually in the range of 20–25% of R_{200} . As a function of redshift, the smallest typical value for angular error is consistently 15% of R_{200} , except for $z < 0.1$, where it is 12%. The largest typical error in angular position increases from 23% of R_{200} for $z < 0.1$ to 32% for $z \geq 0.5$.

As for redshift estimates, the cluster finder assigns a redshift, z_{cl} , according to the kind of redshift measurements available for the galaxies in the cluster. The majority of distant clusters have no galaxies with spectroscopic redshift measurements, so that z_{cl} gets estimated only from

photometric measurements. Here we would like to assess the accuracy of this procedure. To this aim, we analyze errors in estimated cluster redshift, z_{cl} , as obtained from the maximum likelihood procedure by comparing photometric and spectroscopic redshift determinations for the union of two sets of clusters: i) all clusters that have at least five galaxies with spectroscopic measurements (mainly located at $z \leq 0.2$, see fig. 6), and ii) clusters at $z > 0.2$ with at least one of their three brightest members in the r -band having a spectroscopic measurement and $\mathcal{L}_i \geq 1$ (see also WHL). For these clusters we compute the redshift z_p by only using the photometric redshifts of all galaxies. We also compute the redshift estimate z_s from the spectroscopic redshifts, which we make correspond to the BCG redshift in the latter case. These redshift values are then compared to the one obtained using the maximum likelihood method used in the AMF finder (z_{cl}). Results are reported in Table 4 and Figure 7.

We compute $\Delta_z \equiv z_{cl} - z_p$, that is the difference between redshift of the maximum likelihood point (which make use of the spectroscopic redshifts when available) with that obtained from the product of Gaussians using only the photometric redshifts, as a function of redshift bin. We also determine $z_{cl} - z_s$ for each cluster in the sample (see Table 4). For the redshift range where there are many clusters with five spectroscopic redshifts ($z \leq 0.2$), the width of the distribution of differences, $\sigma_{z_{cl}-z_p}$, is about 0.007. For $z \geq 0.2$ we find the width of the distribution to be 0.013, except for the most distant bin ($z > 0.5$), where the width is 0.022. Except for the lowest redshift range ($z < 0.1$), the distribution of differences has an average $|\Delta_z| < 0.002$ and is considered to be unbiased (see Figure 7). For clusters with $z < 0.1$, there is a distinct bias between redshifts determined spectroscopically and those determined photometrically which makes clusters with only photometric redshifts appear $\Delta z \simeq 0.007$ more distant on average. However, of the 838 clusters with $z < 0.1$, 64% have five or more galaxies with spectroscopic redshift measurements associated with them.

We use the width of the distributions, $\sigma \equiv \sigma_{z_{cl}-z_p}$, as a characteristic error for that redshift range and compare $|\Delta_z|$ with 3σ . Over the range $z \geq 0.1$, the percentage of clusters outside 3σ is less than 1.5% per redshift bin. This small percentage of clusters with larger redshift differences is considered to be characteristic of the entire sample, as the distribution of cc2 photometric redshift estimates with $r > 20$ from Oyaizu et al. (2008) mirrors the distribution of spectroscopic redshifts from their sample. No clusters in the $z \leq 0.2$ range have $|z_{cl} - z_s| > \sigma$. From analyses focusing on redshift error versus number of spectroscopic measurements, we know clusters with at least five spectroscopic measurements will have an average error in redshift that is about equal to the velocity dispersion of the constituent galaxies, or $|\Delta z| < 0.002$ with no bias. In all cases, the $z_{cl} - z_s$ is sharply peaked, even for clusters with only one spectroscopic measurement (see dotted lines in Figure 7). Projection effects place a BCG candidate outside of σ in $< 1.7\%$ of the clusters from $z = 0.2$ to $z = 0.5$. For $z > 0.5$, this percentage increases to 2.9%. This analysis allows us to state that $\sigma_{z_{cl}-z_p}$ is a reasonable value to use for the error of the redshift of clusters in each bin.

Table 1. Errors as a function of richness

$\Lambda_{200,min}$	$\Lambda_{200,max}$	Λ_{200}		r_c		position (% of R_{200})	
		Q_1	Q_3	Q_1	Q_3	Q_1	Q_3
100	...	20.2%	23.9%	14.1%	36.0%	6.5%	12.7%
80	100	25.4%	27.6%	19.5%	43.2%	8.2%	15.9%
60	80	28.4%	32.1%	23.0%	51.5%	9.9%	18.0%
50	60	32.1%	35.1%	27.5%	61.6%	11.1%	20.4%
40	50	35.8%	39.6%	32.3%	66.8%	12.5%	22.5%
30	40	39.6%	44.0%	39.1%	74.2%	14.2%	26.3%
20	30	42.5%	50.0%	46.4%	87.3%	17.0%	31.9%

Note. — Ranges are listed for $\Lambda_{200,min} \leq \Lambda_{200} < \Lambda_{200,max}$. Q_1 and Q_3 are the lower and upper quartiles, respectively. The minimum value of r_c in the catalog is 0.059 Mpc, and the maximum value of Λ_{200} is 270.15.

Table 2. Errors as a function of redshift

z_{min}	z_{max}	Λ_{200}		r_c		position (% of R_{200})	
		Q_1	Q_3	Q_1	Q_3	Q_1	Q_3
...	0.1	41.8%	52.3%	74.5%	149%	12.0%	23.0%
0.1	0.2	41.8%	51.5%	64.3%	116%	15.6%	23.8%
0.2	0.3	40.3%	49.3%	49.2%	91.9%	15.3%	26.2%
0.3	0.4	38.8%	47.8%	43.0%	79.7%	15.3%	28.6%
0.4	0.5	38.1%	47.0%	39.5%	74.2%	15.2%	30.3%
0.5	...	38.1%	47.0%	37.9%	69.7%	15.3%	32.4%

Note. — Ranges are from $z_{min} < z \leq z_{max}$. Q_1 and Q_3 are the lower and upper quartiles, respectively.

Table 3. Errors as a function of core radius

$r_{c,min}$	$r_{c,max}$ (Mpc)	Λ_{200}		r_c		position (% of R_{200})	
		Q_1	Q_3	Q_1	Q_3	Q_1	Q_3
...	0.1	45.7%	54.5%	42.2%	71.2%	11.6%	18.2%
0.1	0.2	43.3%	53.4%	45.1%	87.3%	15.0%	25.8%
0.2	0.3	39.9%	51.0%	46.9%	106%	18.1%	32.1%
0.3	0.4	37.5%	48.9%	44.4%	89.7%	18.5%	33.0%
0.4	0.5	35.6%	47.0%	36.9%	70.4%	17.5%	33.2%
0.5	...	32.2%	43.9%	20.2%	43.5%	15.7%	31.6%

Note. — Ranges are from $r_{c,min} < r_c \leq r_{c,max}$ with the same constraints on Λ_{200} and r_c as table 1. Q_1 and Q_3 are the lower and upper quartiles, respectively.

Table 4. Errors in cluster redshift estimates

z_{min}	z_{max}	average offset ($z_{cl} - z_p$)	$\sigma_{z_{cl}-z_p}$	% of clusters with $ z_{cl} - z_p > 3\sigma_{z_{cl}-z_p}$	% of clusters with $ z_{cl} - z_s > \sigma_{z_{cl}-z_p}$	number of clusters in sample
...	0.1	0.0068	0.0070	2.4%	0.0%	543
0.1	0.2	0.0010	0.0074	1.2%	0.0%	1549
0.2	0.3	-0.0003	0.013	1.0%	1.7%	3528
0.3	0.4	0.0005	0.014	0.9%	1.3%	5016
0.4	0.5	-0.0009	0.013	0.5%	1.6%	3533
0.5	...	0.0019	0.022	1.3%	2.9%	557
total	...	0.0003	0.013	0.9%	1.1%	14746

Note. — Ranges are from $z_{min} < z \leq z_{max}$; clusters included in the sample have either five or more spectroscopic redshifts or, for clusters with $z > 0.2$, an associated BCG candidate with a spectroscopic redshift measurement.

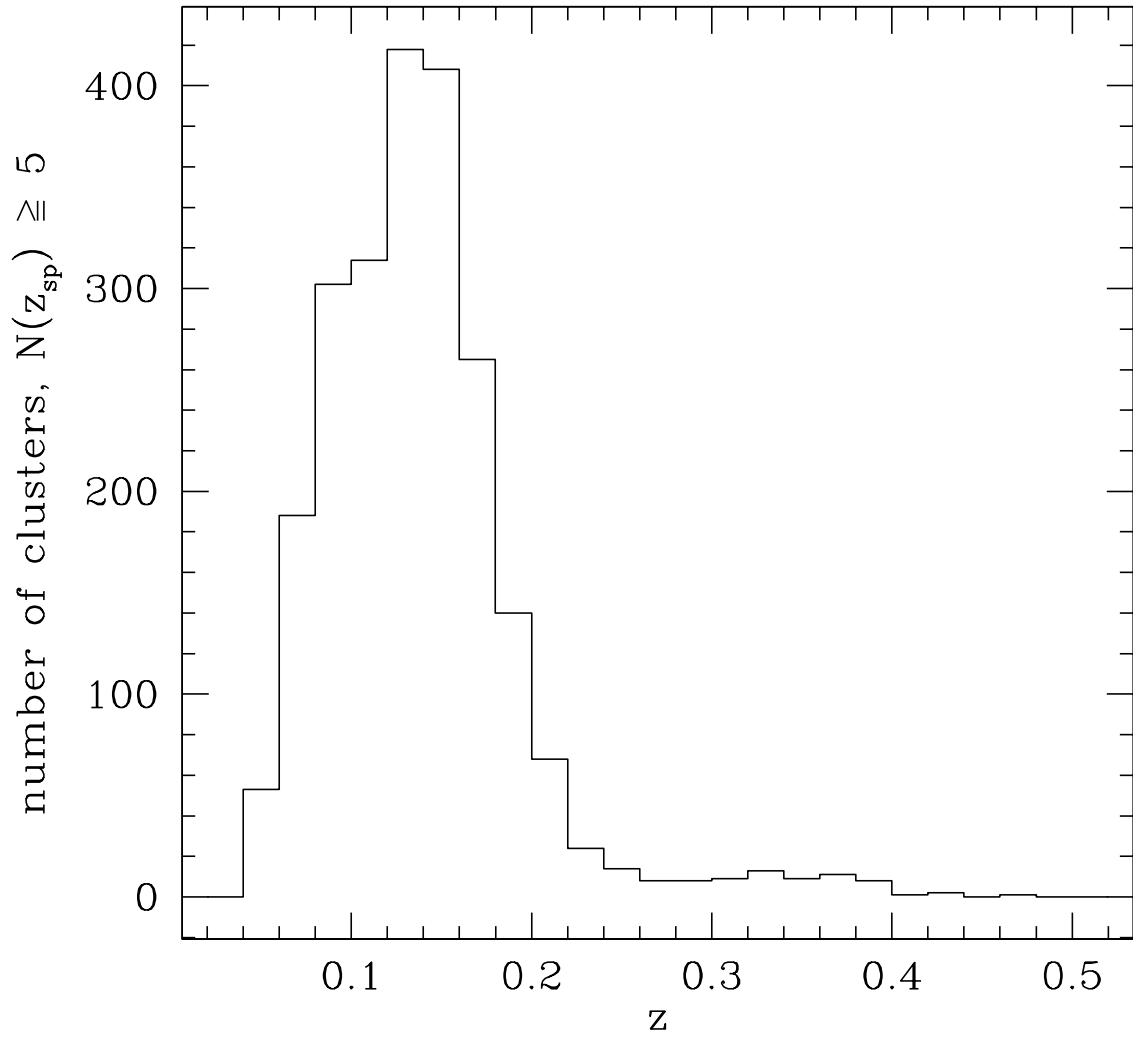


Fig. 6.— Distribution in redshift of clusters that have at least 5 galaxies with spectroscopic redshifts.

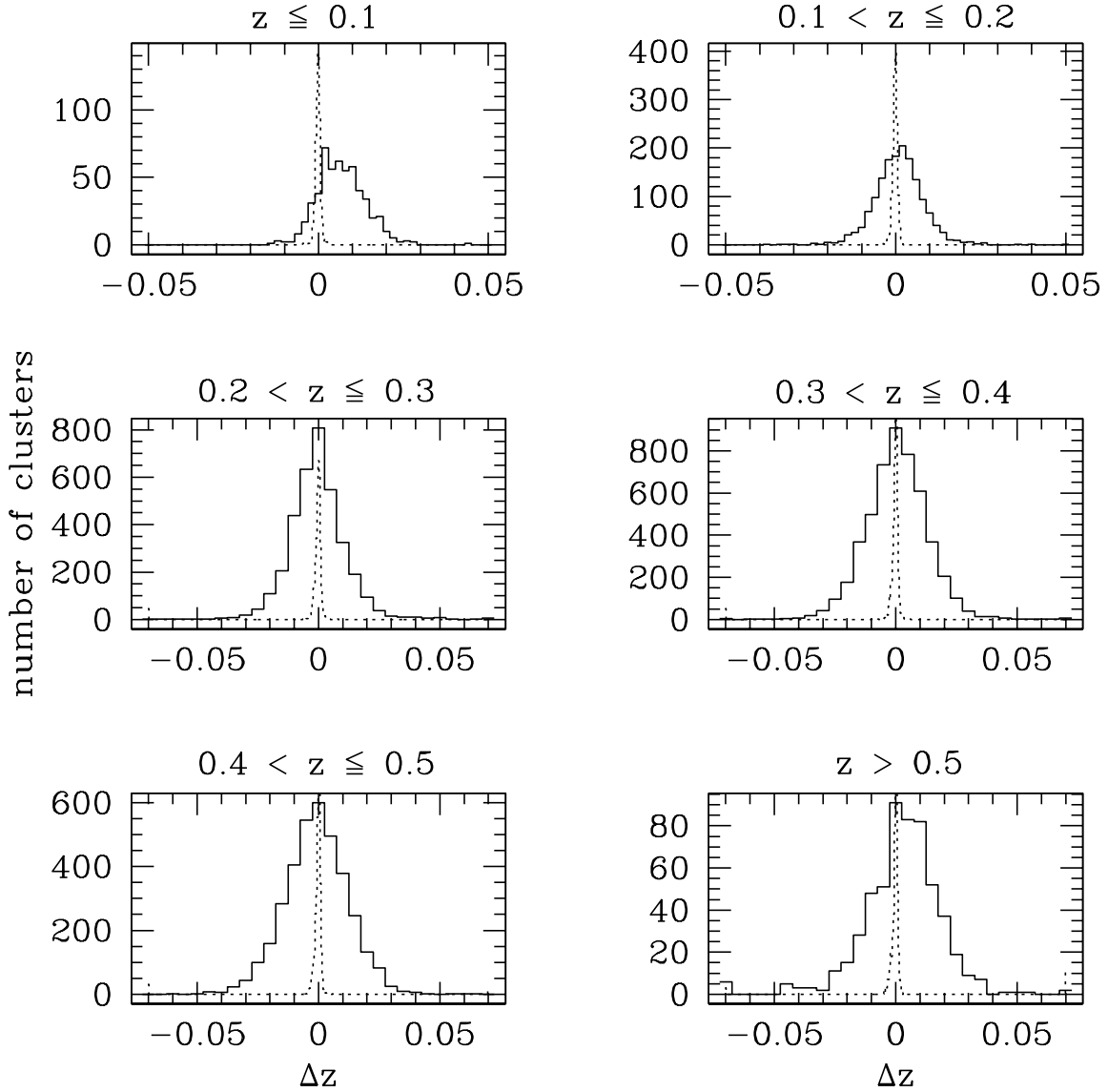


Fig. 7.— Difference between the clusters' redshift realizing the maximum likelihood (z_{cl}) with one obtained from only photometric redshifts (z_p , solid line) and one from only spectroscopic redshifts (z_s , dotted line).

4.3. BCGs in the New Catalog

Since different workers define what they mean by the Brightest Cluster Galaxy somewhat differently, it is not surprising that the assignment of the BCG in a given cluster is not always the same. For this reason we decided to provide a list of the three galaxies that are brightest in the r -band which belong to a specific cluster to aid in comparisons with other catalogs. This list omits galaxies that have no redshift estimate, as those galaxies have a likelihood of being present due to projection effects. The brightest of the candidates is indicated in the list (see Appendix).

We binned the Λ_{200} values for the BCG candidates as shown in table 5 and computed the mean and standard deviation of M^r for both the brightest BCG candidate and for all 3 candidates together. Using $M^r = -2.5\log L_r$, where L_r is the luminosity in the r -band in terms of L^* , we fit $L_r = \beta\Lambda_{200}^\alpha$ and get $\alpha = 0.18\pm 0.01$ and $\beta = 8.4\pm 0.1$.

The evolution of the luminosity of BCGs with respect to redshift has been discussed in numerous papers, most of which assume that the luminosity of the BCG will change with redshift in the same manner that M^* does (Lin & Mohr 2004; Zheng et al. 2005; Hansen et al. 2005; Dong et al. 2008). We examine the evolution of M^r for our brightest BCGs in both redshift and richness in Figure 8. We note that there is an evolution of M^r for any given redshift and any given richness. We also note that the behavior of M^r is flat to a higher redshift for higher richnesses for $\Lambda_{200} < 100$. Thus, for clusters with $\Lambda_{200}=25$, the average luminosity of the BCG is flat to $z \sim 0.2$, whereas for clusters with $\Lambda_{200}=50$, the average luminosity is flat to $z \sim 0.4$. This trend indicates that BCGs in larger clusters formed earlier than BCGs in smaller clusters, thus the more rapid portion of their evolution has ended before $z=0.6$. For clusters with $\Lambda_{200} > 100$ or $z > 0.6$, there are not enough clusters to determine whether the trends established at lower redshifts and richnesses continue.

We also examine the distributions of the difference in redshift between the cluster and the galaxy (Fig. 9). In redshift, the distribution shows a large peak near zero for galaxies with a spectroscopic redshift and a broader Gaussian for those with only photometric redshifts. We find that for the brightest galaxies, there is a bias that assigns photometric redshifts that are too large compared with spectroscopic redshifts for the same galaxy. This bias is reflected in the broad peak of the photometric redshifts in Fig. 9 being shifted by $\Delta z = 0.015$ compared to the spectroscopic peak.

5. Comparisons with Other Catalogs

In order to compare properties such as richness for two different catalogs, it is necessary to determine one-to-one matches for clusters between those catalogs. We match clusters in the AMF catalog with clusters from other catalogs by searching clusters within a given radius and redshift from each AMF cluster center. As for the searching radius, we adopt the AMF R_{200} value of the cluster in hand when comparing with maxBCG, WHL, and GMBCG catalogs, and $1.5 h^{-1}$ Mpc

Table 5. Average M_r as a function of Λ_{200}

$\Lambda_{200,min}$	$\Lambda_{200,max}$	M_r (brightest BCG)	M_r (3 BCGs)
120	...	-23.0 ± 0.7	-22.6 ± 0.6
100	120	-22.9 ± 0.6	-22.5 ± 0.6
80	100	-22.8 ± 0.7	-22.4 ± 0.6
60	80	-22.7 ± 0.6	-22.4 ± 0.7
50	60	-22.6 ± 0.8	-22.3 ± 0.6
40	50	-22.6 ± 0.7	-22.2 ± 0.6
30	40	-22.4 ± 0.7	-22.0 ± 0.6
20	30	-22.3 ± 0.7	-21.9 ± 0.7

Note. — Richness ranges are determined such that $\Lambda_{200,min} \leq \Lambda_{200} < \Lambda_{200,max}$.

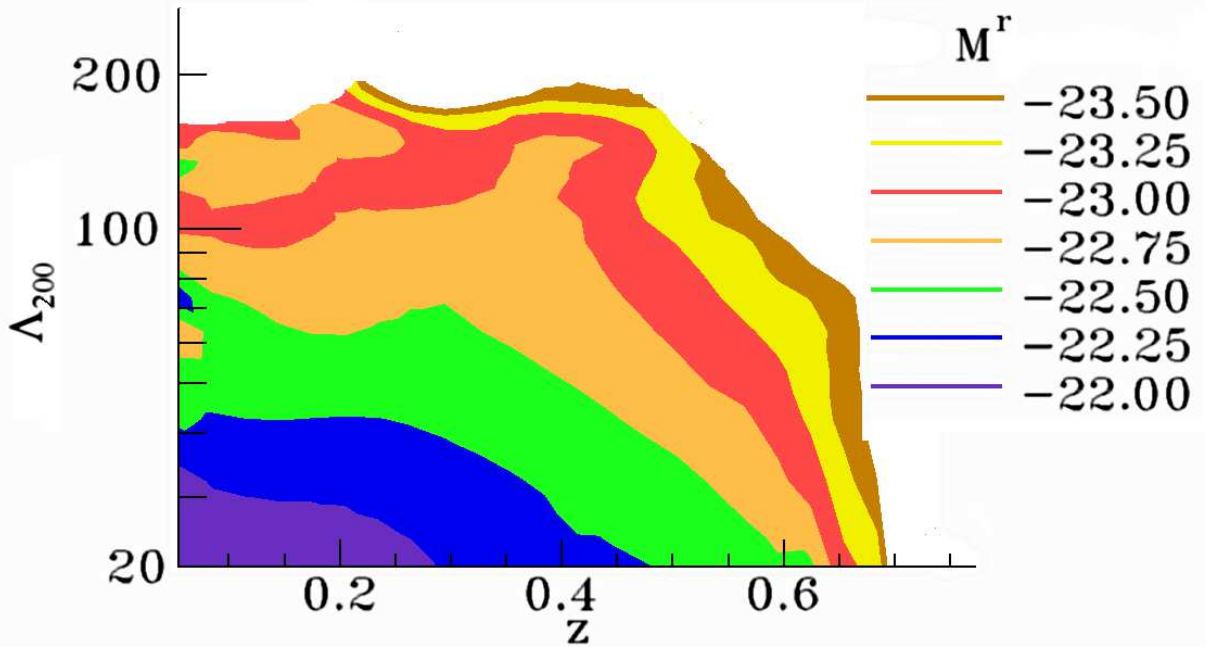


Fig. 8.— Average absolute r -band magnitude vs. redshift and Λ_{200} for the brightest BCG for each cluster. Each contour marks the minimum value of M^r for that region. The magnitudes presented are k -corrected based on the values of z in the AMF catalog using k -corrections as described in Blanton et al. (2003).

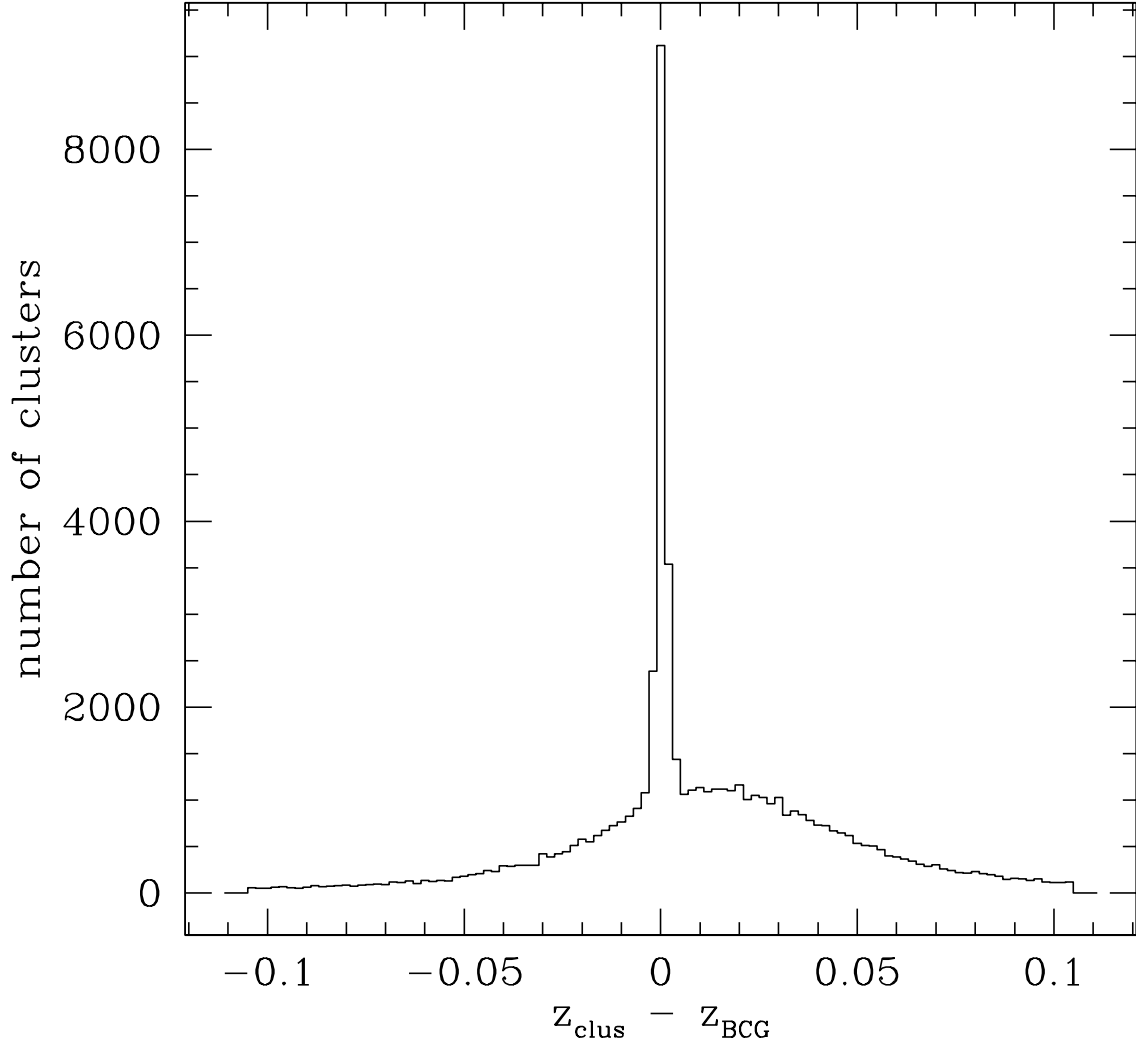


Fig. 9.— Distribution of the difference between cluster redshifts and the redshift of the assigned brightest galaxy; the sharp peak at zero is for BCGs with spectroscopic measurements, and the broader Gaussian is due to BCGs with photometric redshift estimates only. BCGs with no redshift information have been excluded.

when comparing with X-ray data; while we allow for a maximum redshift difference of 0.05. In most cases, clusters in both the AMF catalog and a second catalog are solitary, and there is no need for additional matching criteria. The matches are unambiguous. For the remaining cases, the AMF finder determines several clusters where only one is listed in the other catalog, or, more frequently, the other catalog determines multiple clusters where the AMF catalog lists just one. In these instances, we refine the matching according to the procedure outlined in Appendix C in order to obtain a one-to-one matching between the two catalogs.

One-to-one matches occur in 66% of potential matches between the AMF catalog and the maxBCG catalog, 86% of potential matches between AMF and WHL, 76% of potential matches between AMF and GMBCG, and 60% of potential matches between AMF and our X-ray cluster sample. Additionally, a comparison of the AMF catalog and the Abell catalog finds one-to-one matches for 90% of the AMF clusters in the North Galactic Cap region (stripes 9-39 and 42-44). The minimum z for the AMF finder is 0.045, whereas there is no minimum for the Abell catalog. Of the 1179 AMF clusters matched in the Abell catalog, we measure $z < 0.25$ for 861 (73%) of them.

5.1. Comparison with maxBCG

The most widely used SDSS catalog to date is the maxBCG catalog compiled by Koester et al. (2007). MaxBCG extends over a $\sim 7,500 \text{ deg}^2$ of the $\sim 8,420 \text{ deg}^2$ area covered by the AMF catalog and is restricted to $0.1 \leq z \leq 0.3$. In this region, there are 12,761 AMF clusters between $z=0.1$ and $z=0.3$, and 16,756 AMF clusters between $z=0.08$ and $z=0.33$ (i.e. clusters that might enter the sample due to errors in redshift). The matching procedure defined at the beginning of this section finds 5,447 matches.

Furthermore, using the fact that the given position of a maxBCG cluster is the position of the BCG for that cluster, we identified maxBCG clusters for which the quoted BCG correspond to one of our three brightest galaxies. For unique pairings with cluster redshifts within 0.05 of each other, we found 4317 such BCG matches. We studied the properties of the 1000 maxBCG BCGs which have a geometric match with one of our clusters but do not appear in our BCG list. We found that they are systematically fainter than the AMF quoted BCG, or that one of the AMF BCGs deviates by more than 0.2 mag from the red-sequence.

The separation between centers as a fraction of the AMF cluster R_{200} value is shown in figure 10, showing that a significant fraction of AMF clusters have centers quite distant from the quoted maxBCG one. The histograms for the shared BCG candidates and brightest BCGs keep the same proportion with the curve for those clusters that overlap.

Figure 11 shows the percentages of clusters from one catalog that are matched in the other catalog as a function of redshift, and figure 12 shows this as a function of richness for matches with the maxBCG catalog. Both of the percentage comparisons are based on the 5,447 overlapping

cluster matches. These figures show that the AMF catalog recovers 80% of all maxBCG clusters above $N_{gal} = 80$, but decreases detection to 30% for the smallest maxBCG quoted richness ($N_{gal} = 10$). Similarly, maxBCG finds about 75% of AMF clusters above $\Lambda_{200} = 50$ but drops to 30% detections for $\Lambda_{200} = 20$.

These differences should not be surprising, as the richness criteria for the two catalogs are different. While the AMF catalog relies on the total luminosity within R_{200} , the maxBCG catalog counts any collection of ten or more galaxies that satisfy a luminosity cutoff and color relation as a cluster. The minimum luminosity within R_{200} for one of maxBCG clusters is potentially as small as $4L^*$. In addition, Koester et al. (2007) uses *i*-band values for their luminosity criteria, while we use *r*-band values.

To compare richnesses for matching clusters, we use the $N_{gals}(R_{200})$ value to represent clusters from Koester et al. (2007). Fig. 13 shows the distribution of the richness measurements for each catalog for these clusters using the sample of 5,447 matches. For blended clusters, we always match the maxBCG cluster to the AMF cluster at that site with the highest Λ_{200} value. These are also the clusters on a site with the highest likelihood value. A relationship between the richness values does not become evident until $N_{gals}(R_{200}) \gtrsim 20$. At such richness, the matches between the two catalogs reaches the 50% level. Below this value, the Λ_{200} for a given maxBCG cluster may vary by an order of magnitude. Using the errors on Λ_{200} values as weighting factors, a best fit line to Fig. 13 is

$$\Lambda_{200} = 1.67N_{gals}(R_{200}) + 31.3. \quad (3)$$

The same analysis performed on clusters matched on their BCGs rather than on angular proximity produces a nearly identical relation. For BCG matches, the error-weighted best fit is

$$\Lambda_{200} = 1.61N_{gals}(R_{200}) + 34.8. \quad (4)$$

Note that in both cases the relations are only meaningful for clusters with $N_{gals}(R_{200}) \geq 30$ or $\Lambda_{200} \geq 80$. The errors in Λ_{200} are significantly smaller for larger values of Λ_{200} (see Section 4.2), thus matches with high richness AMF clusters tend to dominate a linear fit.

A thorough comparison aimed at explaining the discrepancies between the two catalogs is quite difficult because not only the two searching methods differ, but also choices on data pre-processing differ. Specific choices on photometric redshifts used, k-correction, band for BCG detection, method for pre-selection of the galaxies to include in the search are all factors that may play a role in the final output. We therefore limited the analysis of the discrepancy to the study of luminosity and color properties of the BCGs for matching clusters and compare them with our whole BCG sample. We computed the offset from the red sequence and the absolute magnitude of BCG (according to the DR6 color frame) in the following BCG samples: *i*) maxBCG BCG for clusters in common between the two catalogs and found among the three AMF brightest galaxies, compared with the brightest AMF BCG for the same clusters. In clusters that AMF and maxBCG share, the maxBCG BCG selection coincides with that of the AMF catalog. Only in 9% of the cases maxBCG misses the brightest galaxy because it is too blue. In such cases maxBCG uses the 2nd or the 3rd as

seed for the cluster. The fraction of blue BCG found here is consistent with what is found for rich systems ($\Lambda_{200} > 50$) in the whole AMF catalog (6.2%, see Pipino et al. (2010), fig. 2). *ii*) maxBCG BCG for clusters in common between the two catalogs, compared with AMF first ranked BCG for all AMF clusters below $z \leq 0.3$. An increase in the tail of blue BCG in the AMF catalog is apparent, now amounting to 15.8% of the cases. Note that 14.6% is the fraction of blue first ranked galaxies in all AMF clusters. AMF BCGs are also slightly fainter than maxBCG ones, because here we are including in the comparison several clusters that don't match with maxBCG ones. *iii*) first ranked AMF BCGs in the redshift range $0.1 \leq z \leq 0.3$ that are not in clusters that share the BCG with maxBCG. The AMF BCGs in this case are on average fainter (as we tend to retain here only poor systems) and the fraction of blue BCG goes up to 16%. The existence of such blue BCGs in our sample is intriguing, and it would be important to further confirm it with spectroscopic studies of this sample.

While the differences in colors between the AMF and maxBCG BCGs are evident, they don't seem to be sufficient to explain the quite substantial differences between the two catalogs. It is possible that the biggest difference in the low luminosity end of the two catalogs is due to maxBCG requiring clusters to have at least ten ridgeline galaxies found in the proximity of the selected BCG. These color cuts reduce the number of galaxies in the input SDSS photometric database to one fifth with respect to the initial value.

A search for max BCG clusters in an extended AMF catalog also retaining systems with richness in the range $12 \leq \Lambda_{200} < 20$ leads to a 33% increase in the number of matches, from 6000 to 8000 matches. However, the completeness of the cluster finder is $\sim 50\%$ for this size cluster (D08). Thus, it is possible that this increase of 33% represents only half of the matches gained by lowering the minimum Λ_{200} value, *i.e.* the actual gain is 66%, or 10,000 matches. As we lower the threshold further, the completeness decreases, making comparisons even more difficult.

Koester et al. (2007) report the total luminosity in the r -band of the members of their clusters as L_r^{memb} . By accounting for the evolution of L^* with redshift for our clusters, we can make a direct comparison of our Λ_{200} values with their L_r^{memb} values. The range for $20L^*$ for z between 0.1 and 0.3 for our catalog is 38 to $50 \times 10^{10} L_\odot$. There are only ~ 1600 maxBCG clusters with $L_r^{memb} \geq 40 \times 10^{10} L_\odot$. Because we know we match at least 5000 of their clusters based on BCG, our clusters match with maxBCG clusters whose luminosity in the r -band is less than our richness cutoff of $20L^*$. A large percentage of maxBCG clusters are likely to be too poor to be detected by our finder.

5.2. Comparison with WHL Clusters

The WHL catalog (Wen et al. 2009) was produced from the same SDSS Data Release as our catalog. The angular positions provided by Wen et al. (2009) are of the BCGs of their clusters. The following comparisons are for cases where the WHL BCG lies within our value of R_{200} from the

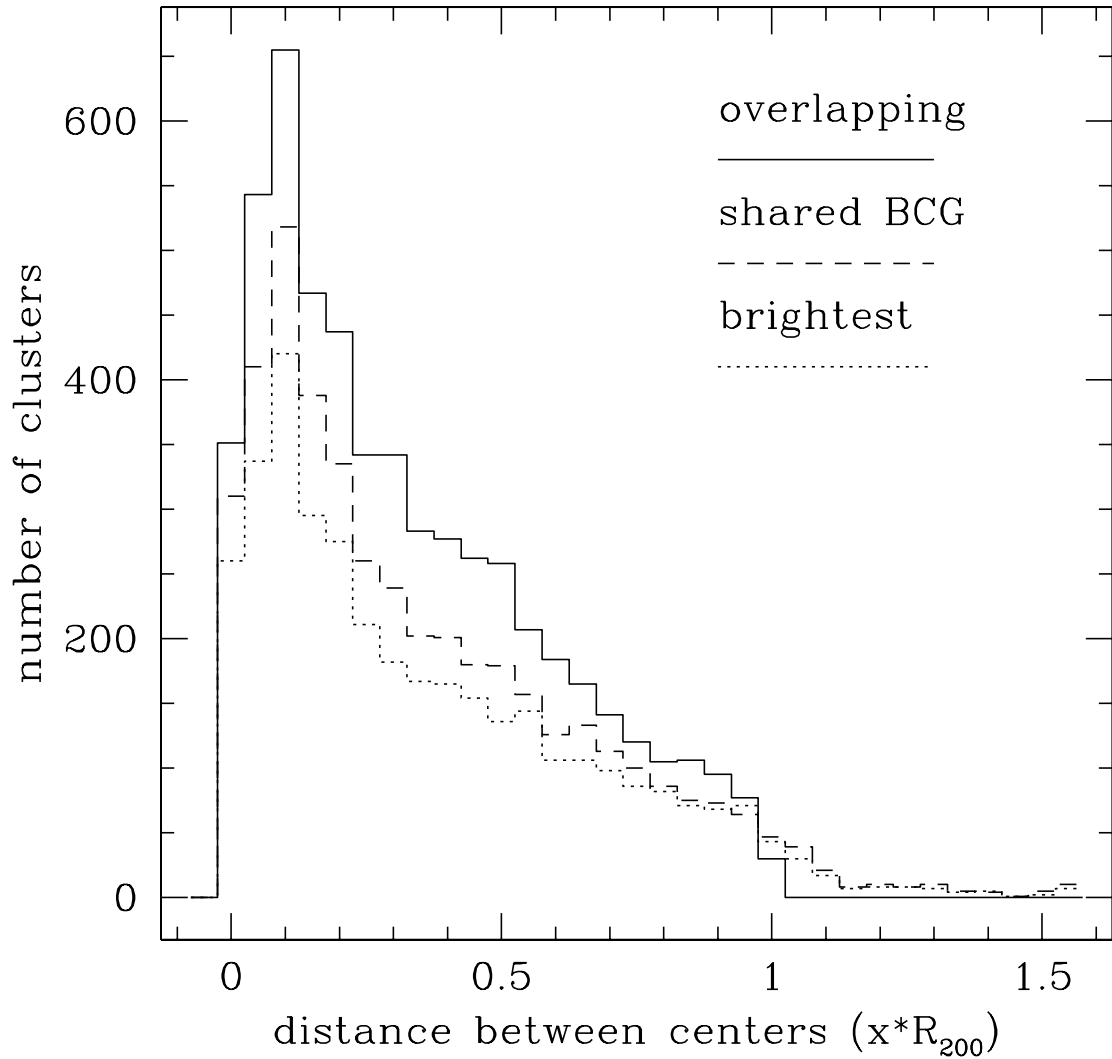


Fig. 10.— Separation between AMF and maxBCG cluster centers for clusters whose centers are within R_{200} of the AMF cluster (solid line), those which also share a BCG candidate from our catalog (dashed line), and those where our brightest BCG candidate matches the maxBCG BCG (dotted line).

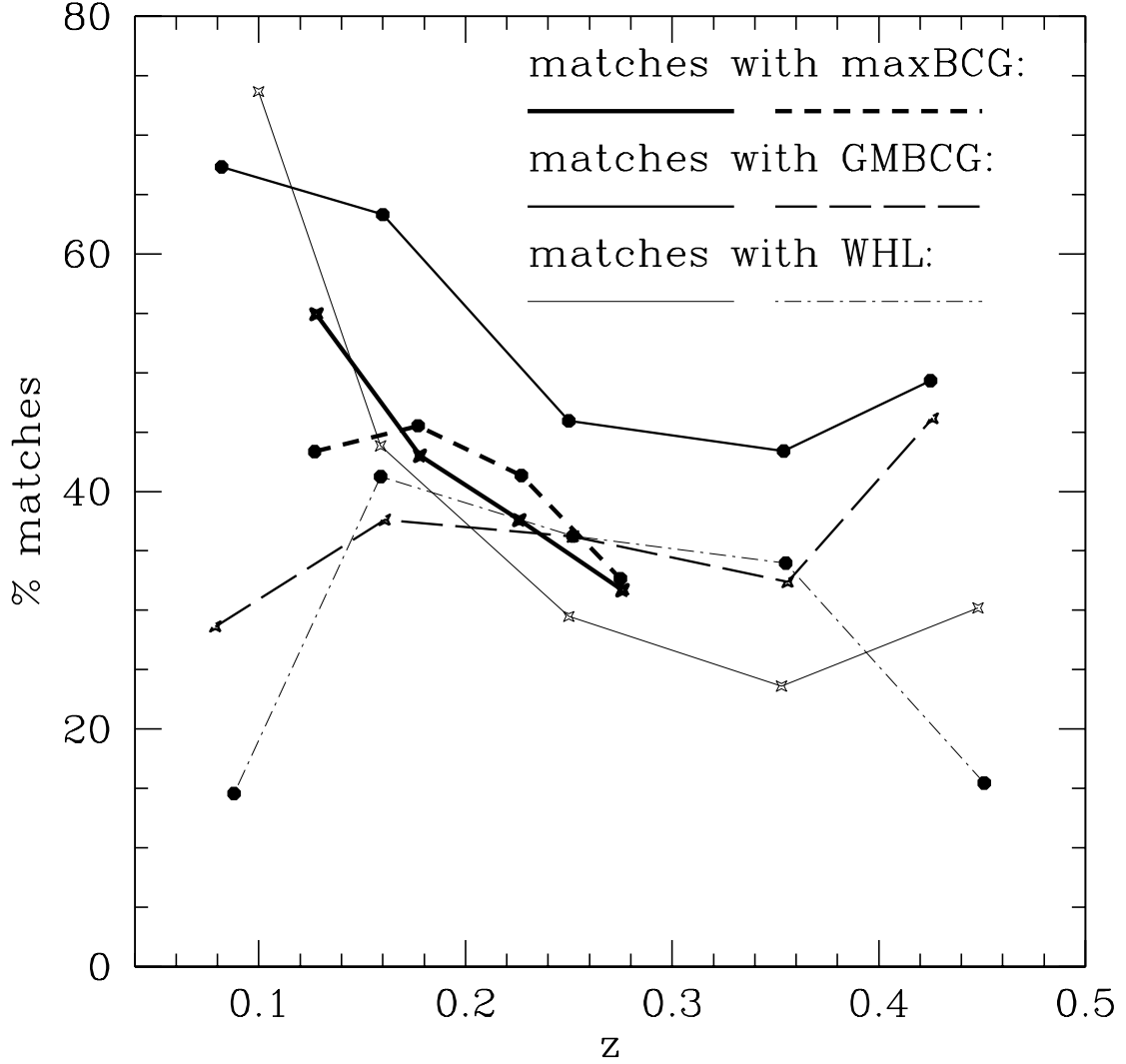


Fig. 11.— Percentage matches between the AMF catalog and other catalogs by redshift bin; the solid line represents the percentage of clusters from the other catalog matched with an AMF cluster, and the segmented line shows the percentage of AMF clusters matched with with a cluster in the other catalog. The heaviest line and dotted line represent maxBCG matches. The medium line and dashed line represent GMBCG matches. The thinnest line and dashed-dotted line represent WHL matches.

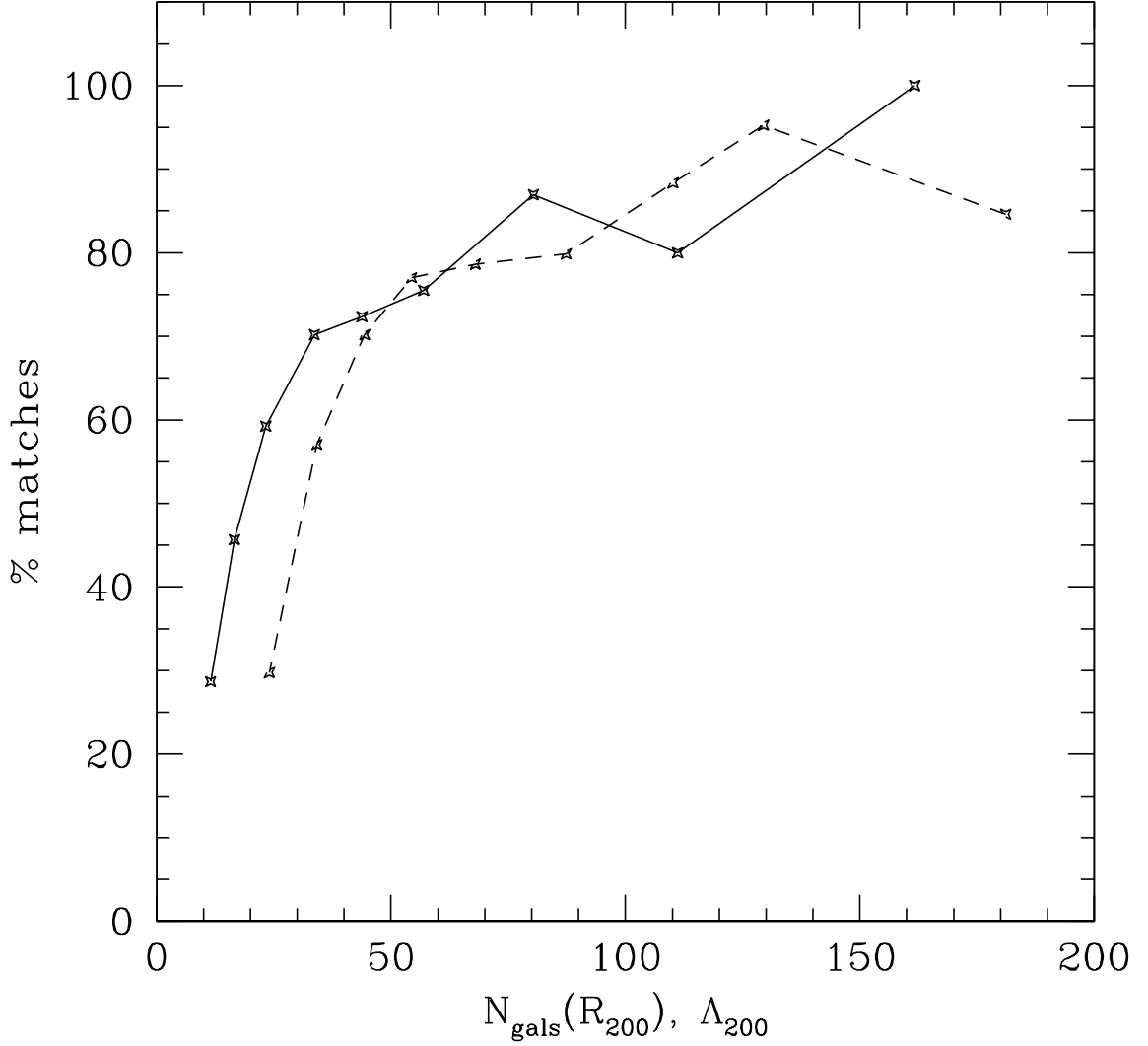


Fig. 12.— Percentage of the matches between the AMF catalog and the maxBCG catalog as a function of richness; the solid line shows the percentage of maxBCG clusters that have an AMF match as a function of $N_{\text{gals}}(R_{200})$; the dashed line indicates the percentage of AMF clusters in the $0.1 \leq z \leq 0.3$ range with a maxBCG match as a function of Λ_{200} .

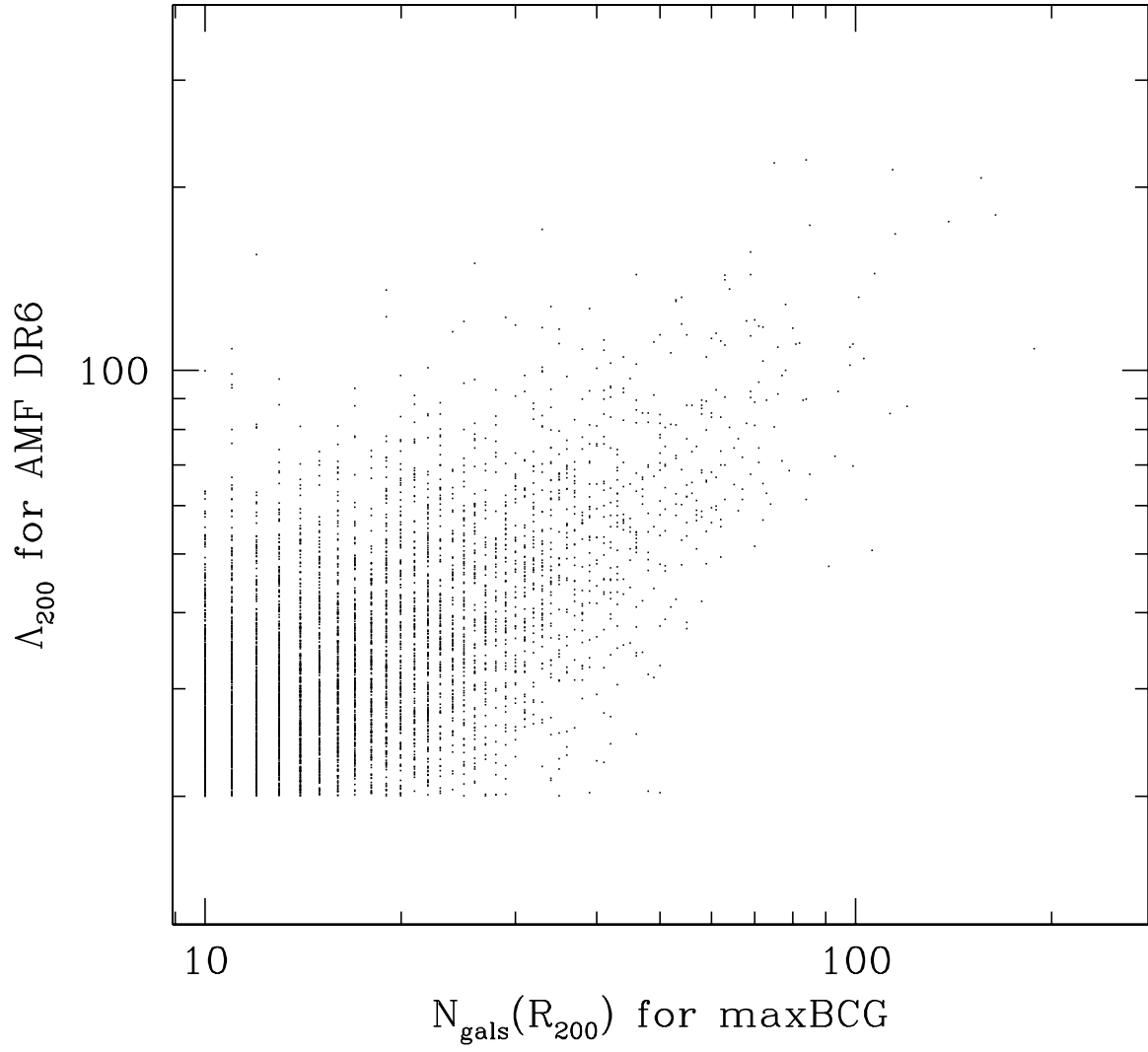


Fig. 13.— Λ_{200} vs. $N_{\text{gals}}(R_{200})$ for matching clusters.

center of our cluster, and $|\Delta z|$ between the photometric redshift of their cluster and the redshift of our cluster is ≤ 0.05 . We find 17,579 pairs, or matches for slightly less than 50% of their clusters. As with the maxBCG comparison, the method of cluster identification along with the completeness of the surveys for smaller cluster sizes will affect the number of matches. Figure 14 shows the distribution of separations of our cluster centers and the WHL BCGs. The peak in separations with this binning occurs at a difference of $0.1 \text{ h}^{-1} \text{ Mpc}$ — the same value as the comparison with maxBCG clusters. Figure 15 shows the distribution of redshift differences between matching clusters. There is a slight ($\Delta z = 0.006$) bias toward AMF clusters being more distant; most paired clusters lie within $|\Delta z| = 0.025$ of each other, which is to be expected considering the error in redshift measurements for each finding technique. To compare sizes of paired clusters, we examine how our Λ_{200} value compares with the richness reported by Wen et al. (2009) in Figure 16. The amount of scatter has decreased with respect to the maxBCG comparison (Figure 13). The error-weighted least-squares fit to the data gives

$$\Lambda_{200} = 3.79R + 13.7. \quad (5)$$

In Figures 11 and 17, we examine the relative completeness of the AMF and WHL catalogs in redshift and richness with respect to each other. The WHL catalog has matches in the AMF catalog for $>70\%$ of its clusters with $R \geq 25$. The percentage of WHL clusters with matches in our catalog increases to $>80\%$ for its richest clusters. The completeness of AMF clusters which have matches in the WHL catalog follows a different trend. For $20 \leq \Lambda_{200} \leq 100$, the percentage of matches increases from $<20\%$ to just under 70%. Above $\Lambda_{200} = 110$, the percentage of matches falls to between 55 and 60%. In some cases, our larger clusters are fragmented into several smaller clusters in the WHL catalog, and our lists of matching pairs do not identify one-to-one matches in this case. In redshift, Figure 11 shows that most of the WHL clusters nearer than $z = 0.2$ have matches in the AMF catalog ($>60\%$). To the contrary, there are $<40\%$ matches in the WHL catalog for AMF clusters over the entire redshift range. This can be attributed to the fact that we find more clusters overall.

5.3. Comparison with GMBCG

The GMBCG catalog (Hao et al. 2010) is the follow-up to the maxBCG catalog. It employs a more sophisticated method for determining the magnitude versus redshift distribution and extends the range from a maximum of $z = 0.3$ (for maxBCG) to a maximum of $z = 0.55$. This catalog still displays a richness distribution similar to the maxBCG catalog in that it finds many objects that are below the detection threshold of the AMF catalog.

There are 15,214 one-to-one matches between the AMF and GMBCG catalogs in the region of the sky where the catalogs overlap and for $z \leq 0.55$. The GMBCG catalog does not detect clusters in regions that were not covered by DR6, nor does it include the portions of stripes 38 and 39 with

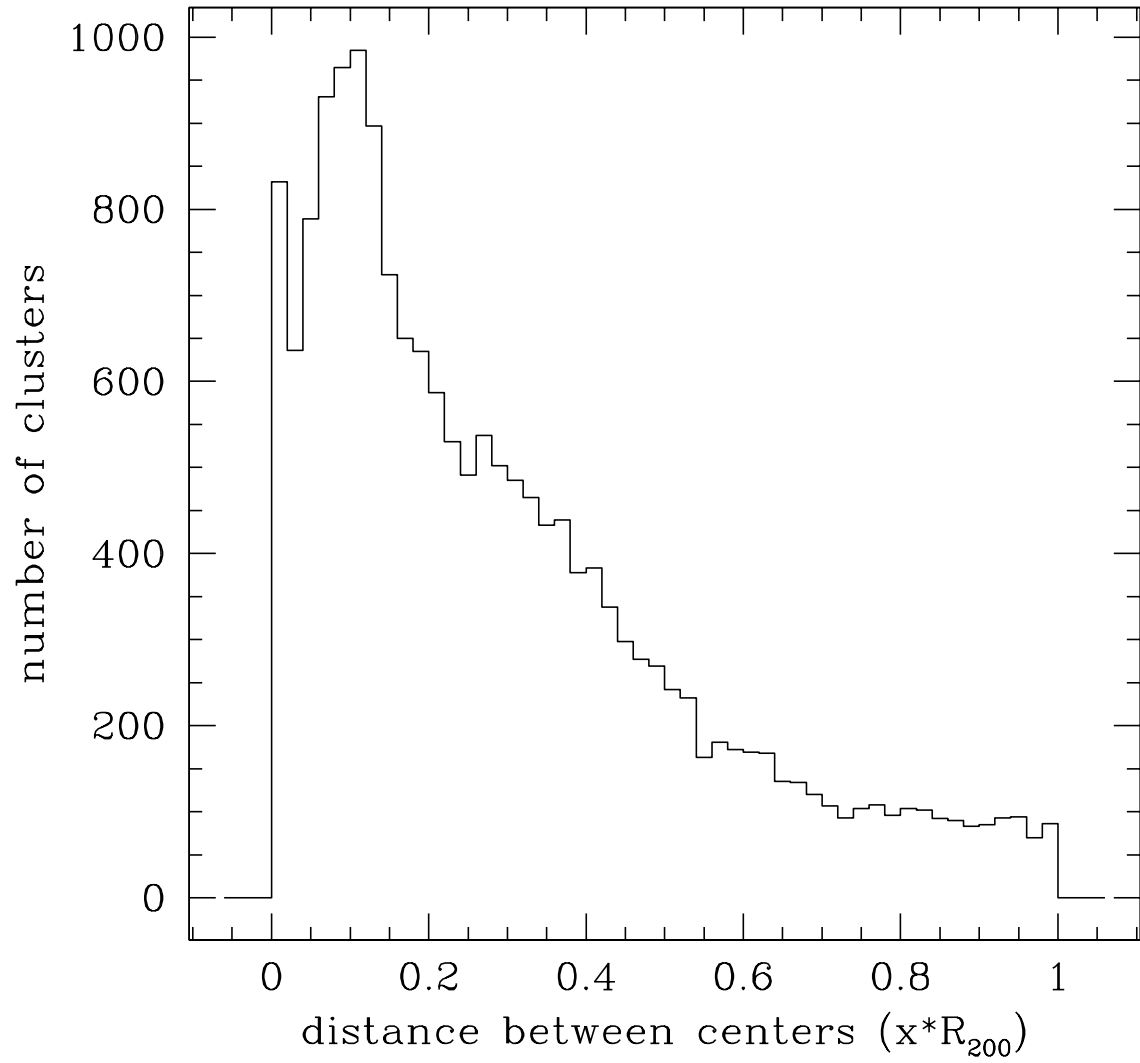


Fig. 14.— Distribution of separations between the AMF cluster centers and WHL BCGs for matching clusters.

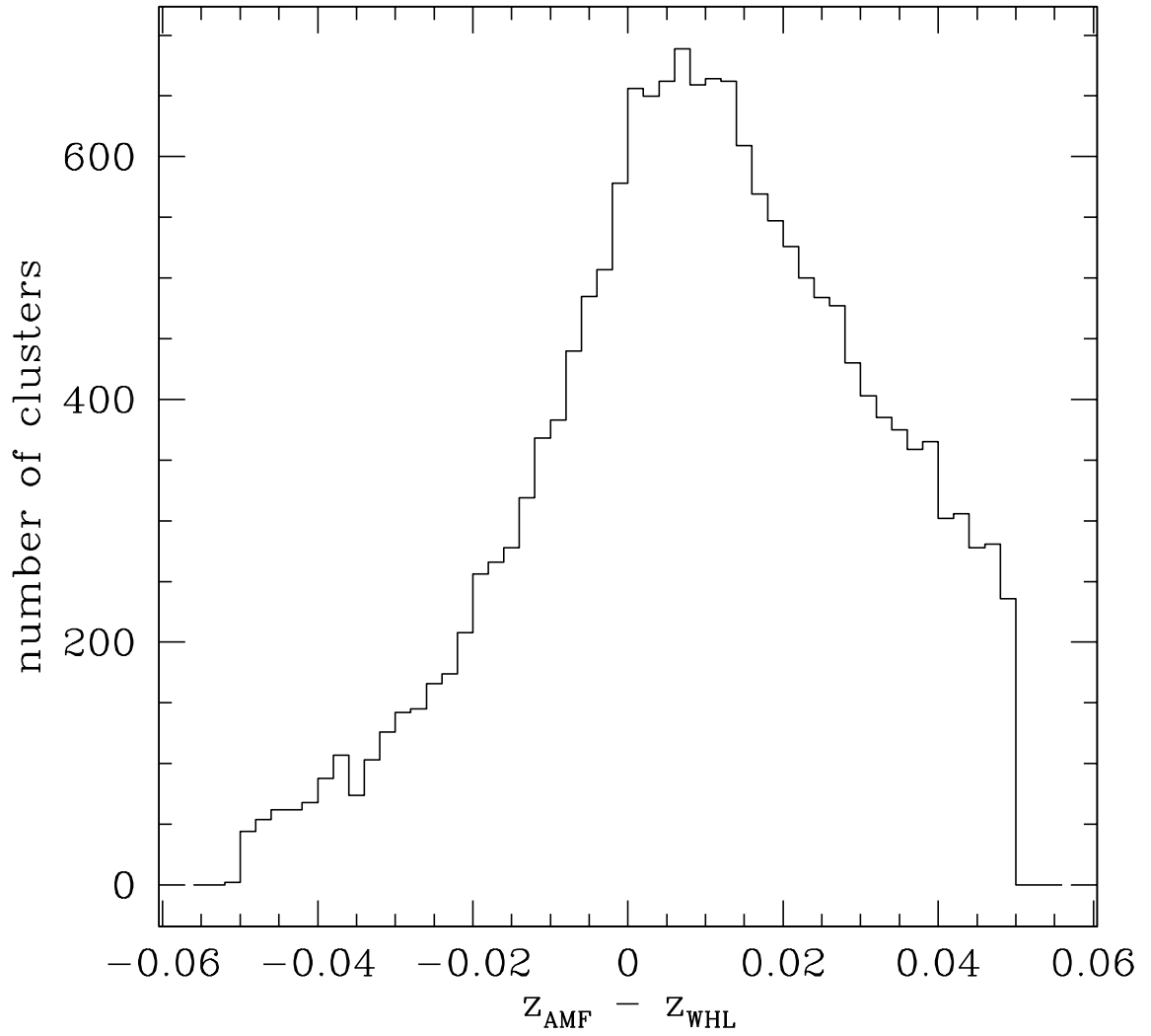


Fig. 15.— Distribution of Δz values for matching AMF and WHL clusters.

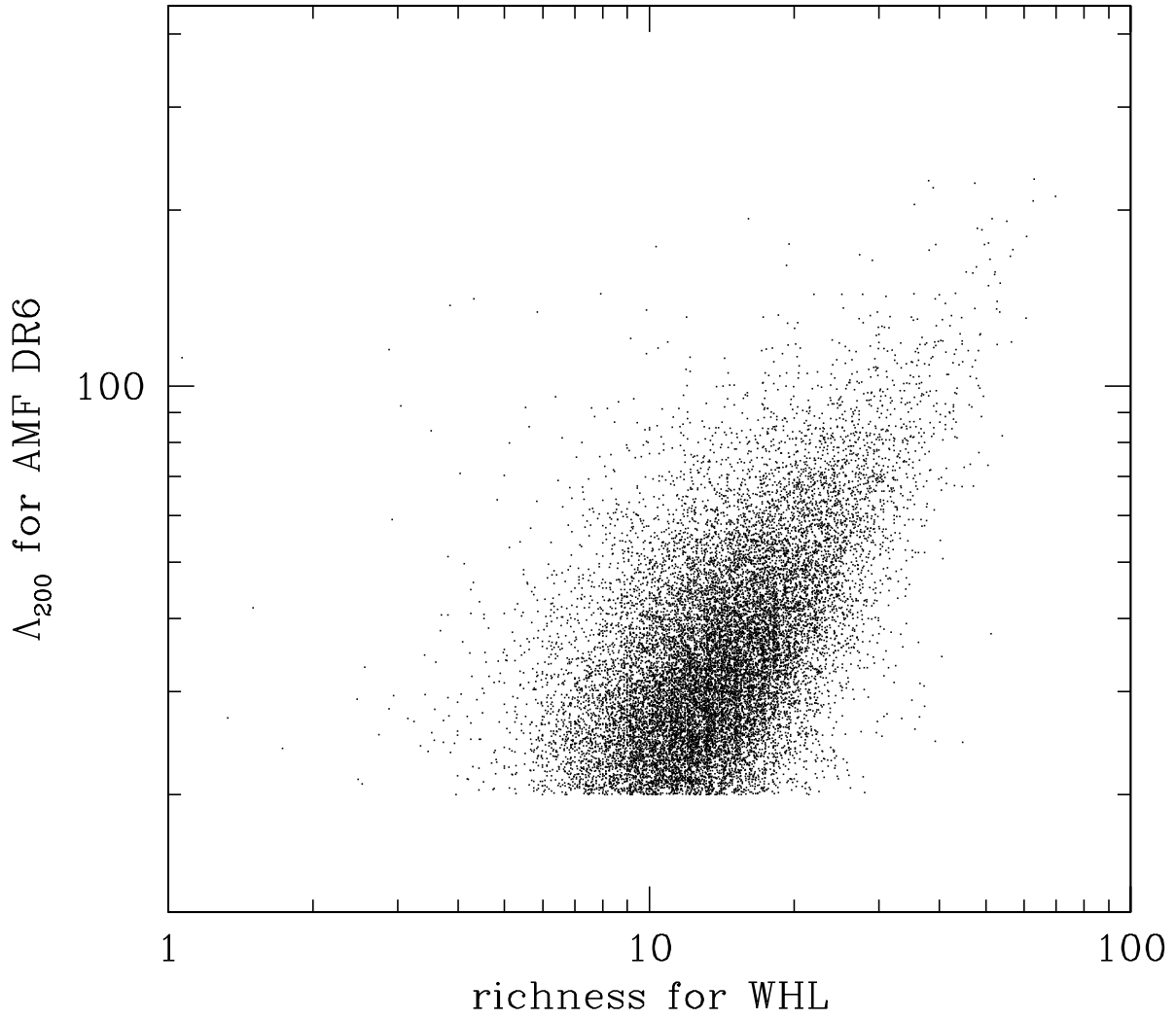


Fig. 16.— Λ_{200} values (AMF) vs. richness values (WHL) for paired clusters.

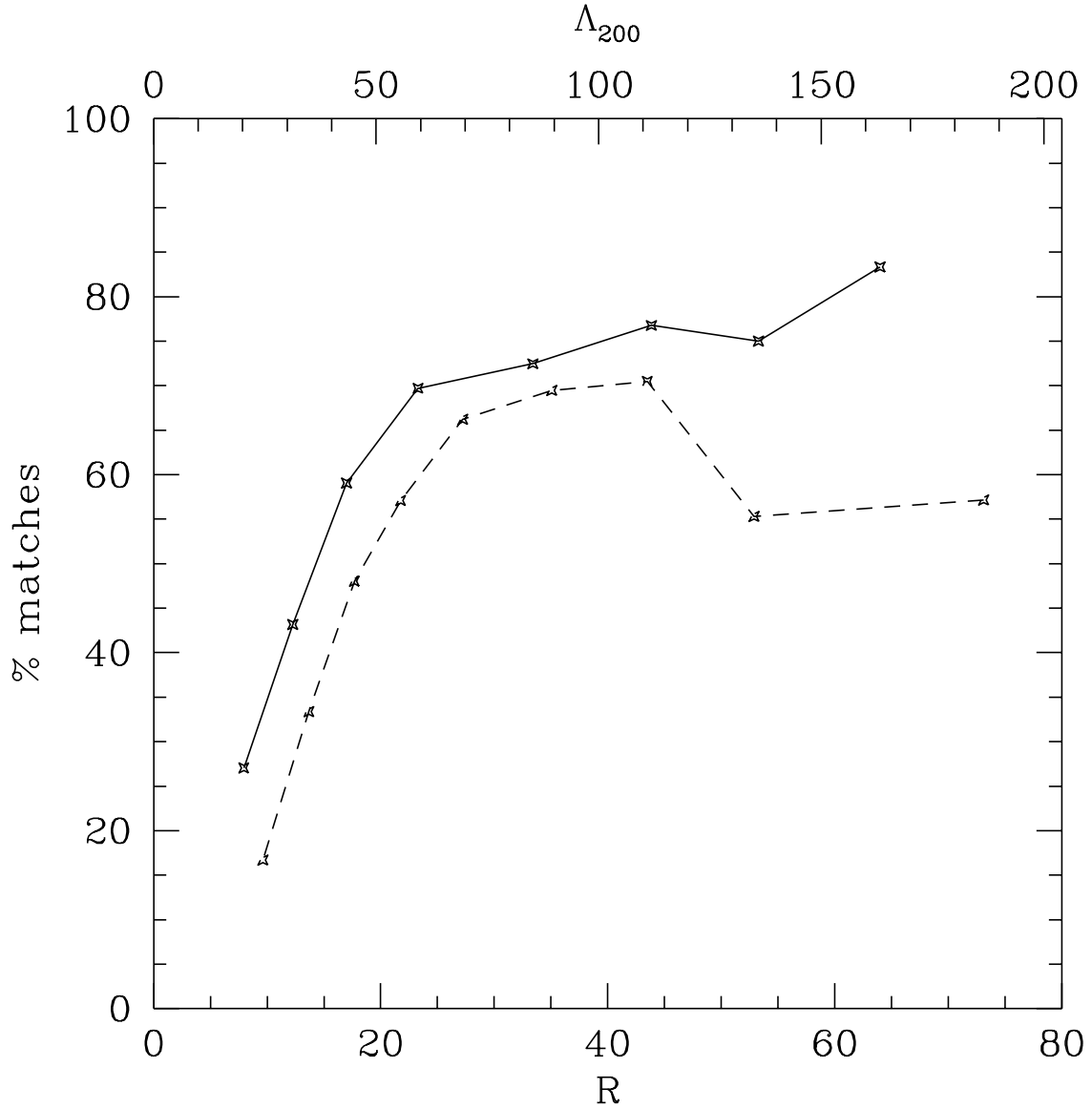


Fig. 17.— Percentage of the matches between the AMF catalog and the WHL catalog as a function of richness; the solid line shows the percentage of WHL clusters that have an AMF match as a function of R (lower x-axis); the dashed line shows the percentage of AMF clusters in the $z \leq 0.6$ range with a WHL match as a function of Λ_{200} (upper x-axis).

RA > 200° or stripe 44. Figure 19 shows the distribution in matching clusters as a function of $z_{AMF} - z_{GMBCG}$. More than 5,000 of the matching clusters have a $|\Delta z| \leq 0.005$.

For one-to-one matching clusters, we plot the value of Λ_{200} vs. the value of N_{gals} in figure 20. We use the weighted value of N_{gals} if the `WeightOK` flag is set, otherwise we use the richness from `GM_Scaled_Ngals`. Using the errors on Λ_{200} values as weighting factors, a best fit line to Fig. 20 is

$$\Lambda_{200} = 1.37N_{gals}(R_{200}) + 47.8. \quad (6)$$

As the errors are smaller for richer AMF clusters, the fit is biased toward larger clusters.

Figure 11 shows the percentage of clusters in one catalog that are matched in the other as a function of redshift. Figure 21 represents the percentage of the AMF and GMBCG catalogs in richness which have matches in the other catalog. For $\Lambda_{200} > 80$ for AMF clusters and $N_{gals} > 55$ for GMBCG clusters, the catalogs have 60% of their members matched in the other catalog, except for the highest richness clusters in the GMBCG catalog that match more than 70% of clusters in the AMF catalog. The richest clusters in the AMF catalog are often fragmented into multiple smaller clusters in the GMBCG catalog. The issue of clusters the GMBCG catalog having many clusters below the richness threshold used for the AMF catalog is the same issue we examined when comparing our catalog to the maxBCG catalog in section 5.1. This results in many of our richest clusters not having a one-to-one match with a GMBCG cluster.

5.4. Comparison with X-ray Clusters

In order to find a X-ray counterpart to clusters in our catalog we retrieved data from different sources and created an input list for a cross-matching procedure. The vast majority of the clusters in such list comes from the X-ray Clusters Database (BAX) as available on 24 June 2009. A BAX query returns nearly 1000 clusters and groups in the region of the sky covered by DR6. Luminosities for the BAX objects have been recalculated in order to reflect the cosmology assumed in this paper. Another 26 clusters from very recent papers in the literature (Balestra et al. 2007; Maughan et al. 2008; Cavagnolo et al. 2009) have also been added to the list. These works also provided (updated) temperature measurements. While this compilation comprises the widest possible set of X-ray clusters we can match, it is not a well defined sample in terms of characteristics. We therefore also match our AMF sample with the flux-limited NORAS catalogs in the overlapping regions.

The cross-matching procedure is performed in spatial position and redshift. In particular, we match the BCG position in our catalog to the quoted X-ray center, which is typically separated by less than 100 kpc (Lin & Mohr 2004; Cavagnolo et al. 2009, e.g.). We match 539 clusters from the input list, with the vast majority showing agreement between the BCG position and the X-ray center within $0.5 \text{ h}^{-1} \text{ Mpc}$ (Fig. 22). Among those, 505 are nearer than $z = 0.4$. As for NORAS, we match 155 clusters among which 150 have a redshift below $z = 0.4$. The richness and redshift distribution of the matching clusters are reported in Figs. 23 and 24.

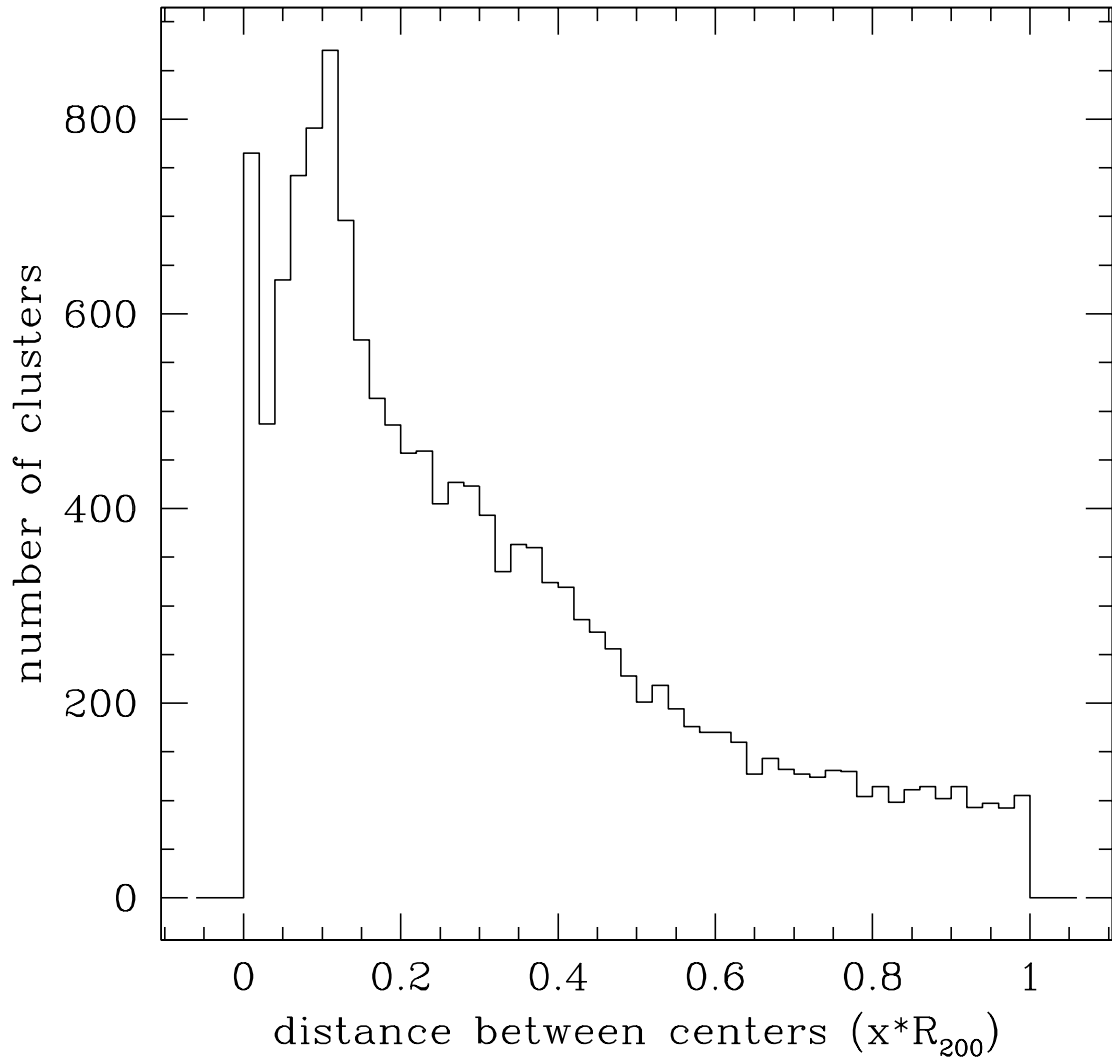


Fig. 18.— Distribution of separations between the AMF cluster centers and GMBCG BCGs for matching clusters.

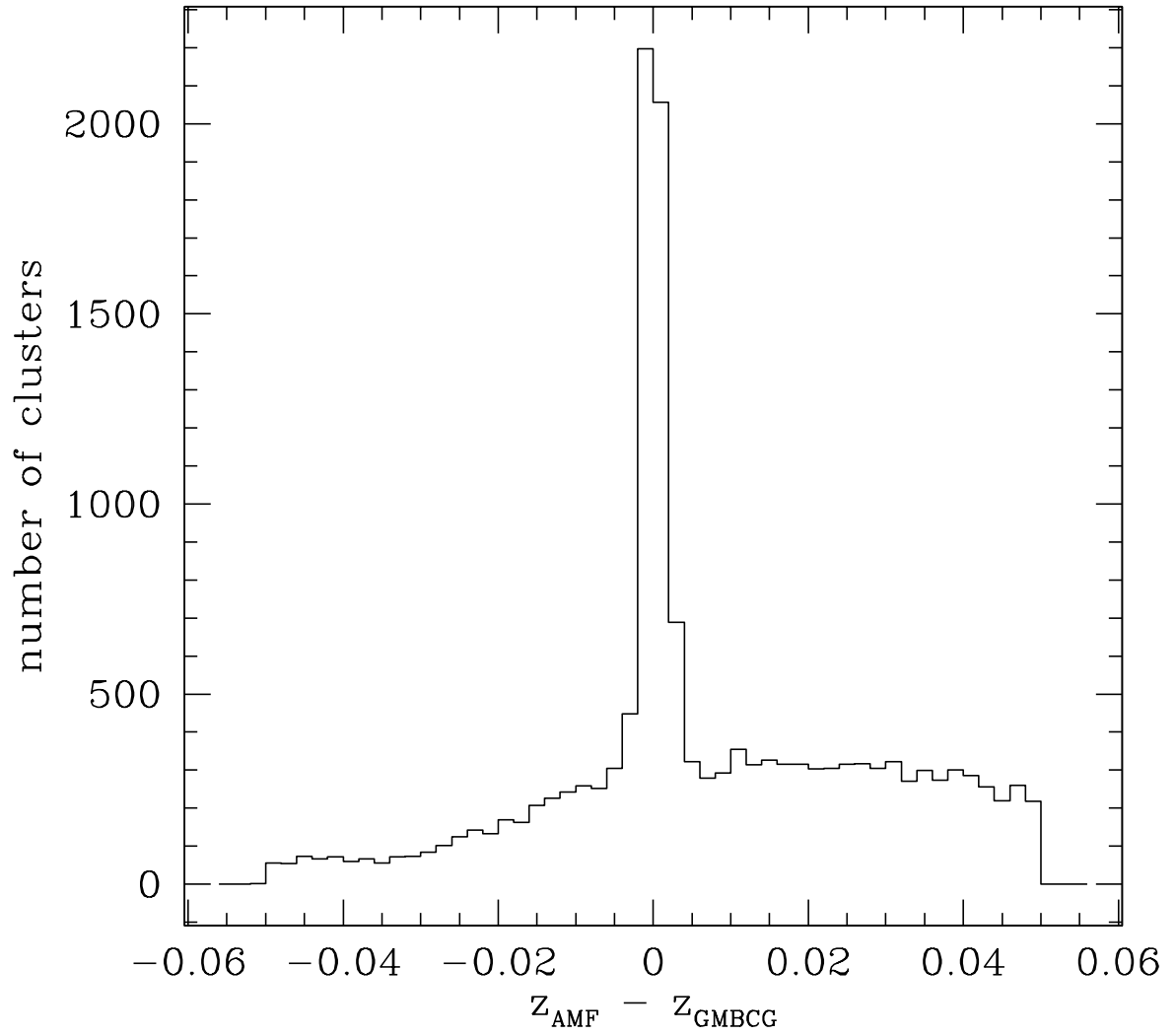


Fig. 19.— Distribution of Δz values for matching AMF and GMBCG clusters.

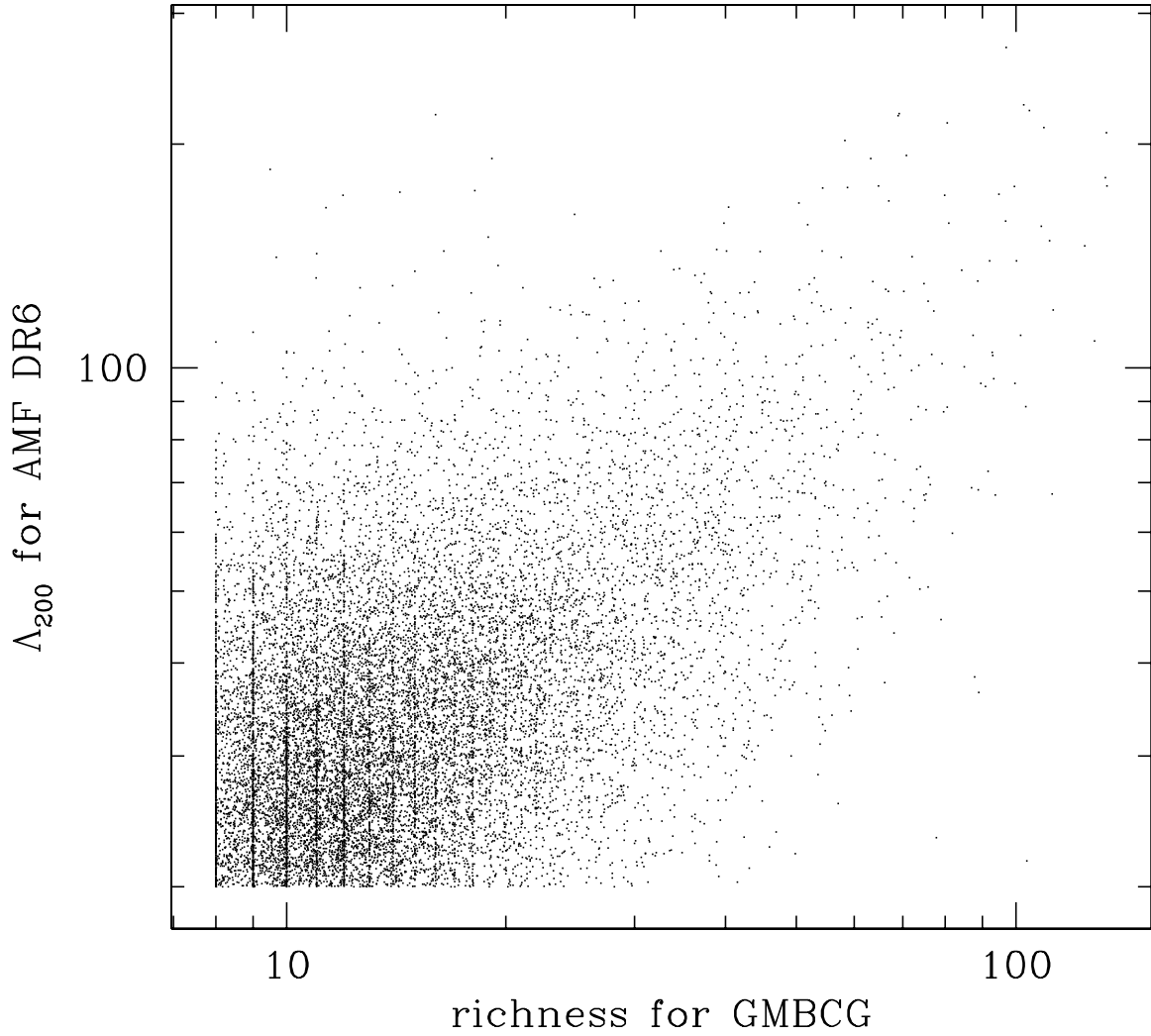


Fig. 20.— Λ_{200} values (AMF) vs. richness values (GMBCG) for paired clusters. The richness from the GMBCG catalog is the weighted value of N_{gals} if the `WeightOK` flag is set; otherwise, the scaled value of N_{gals} is used.

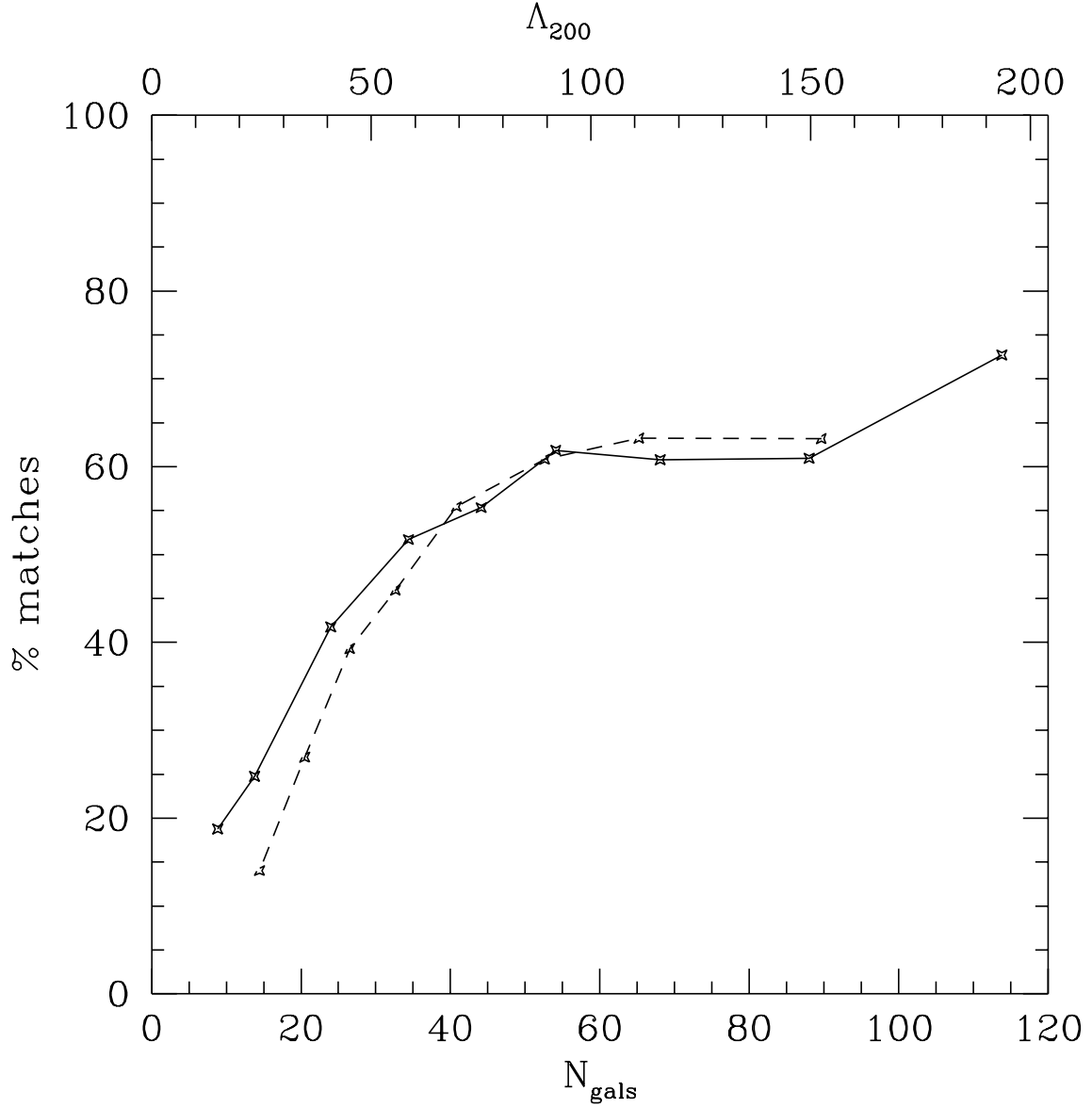


Fig. 21.— Percentage of the matches between the AMF catalog and the overlapping sections of the GMBCG catalog as a function of richness; the solid line shows the percentage of GMBCG clusters that have an AMF match as a function of N_{gals} (lower x-axis); the dashed line shows the percentage of AMF clusters in the $z \leq 0.55$ range with a GMBCG match as a function of Λ_{200} (upper x-axis).

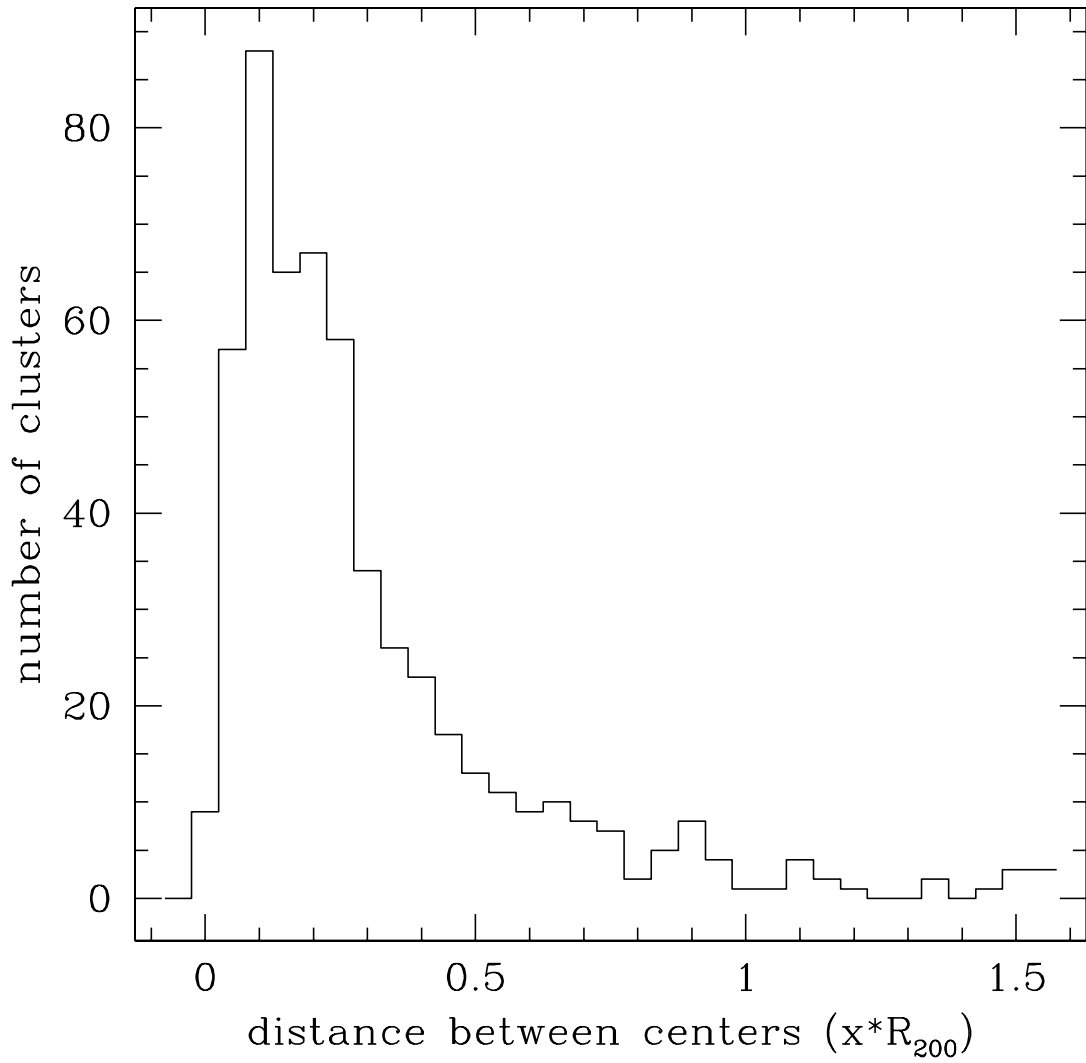


Fig. 22.— Distance between the center of the AMF cluster and the center of the BAX cluster as a fraction of R_{200} of the AMF cluster.

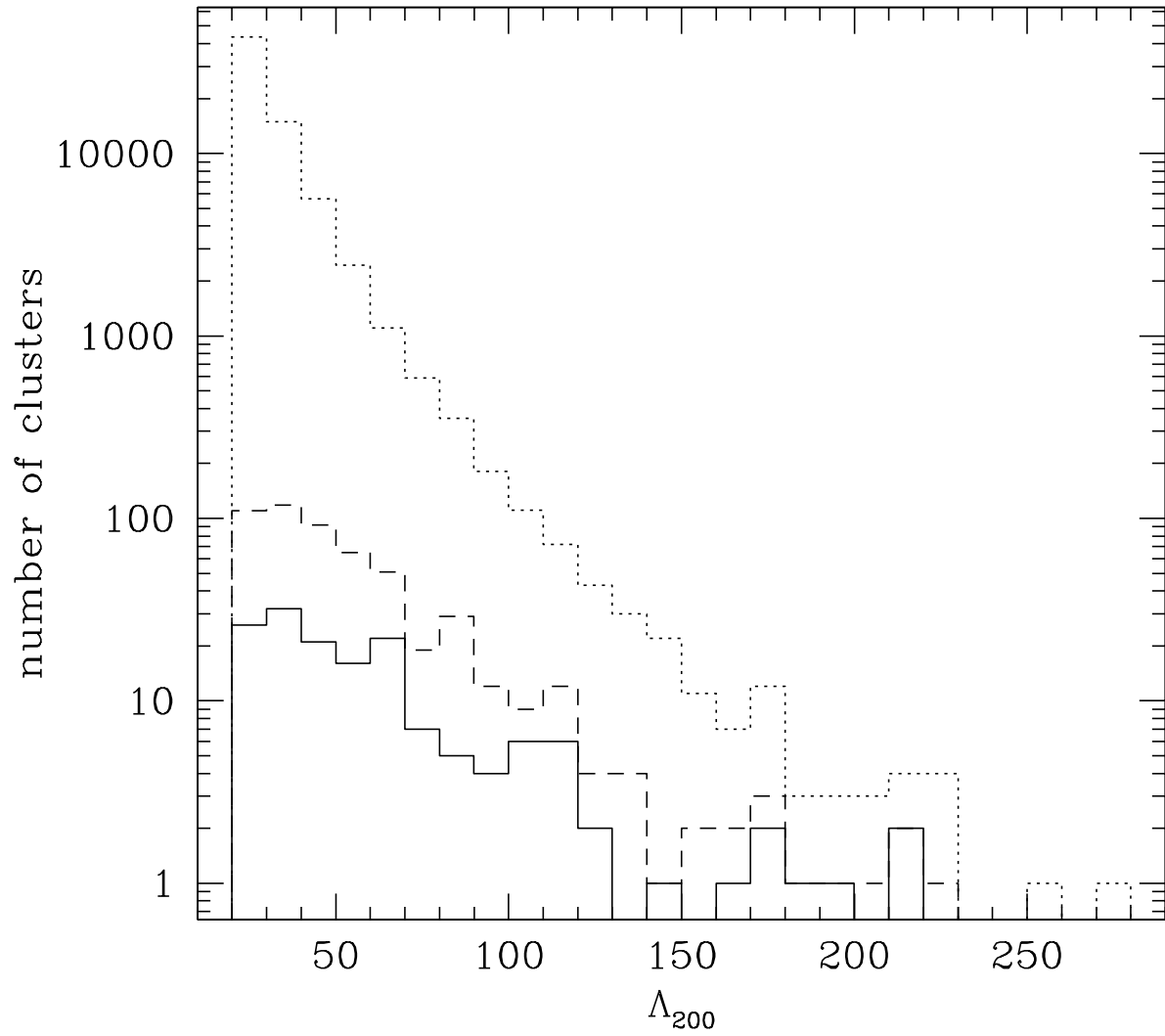


Fig. 23.— Number of matching clusters as a function of Λ_{200} ; dotted line: all AMF DR6, dashed: BAX matches, solid: NORAS matches.

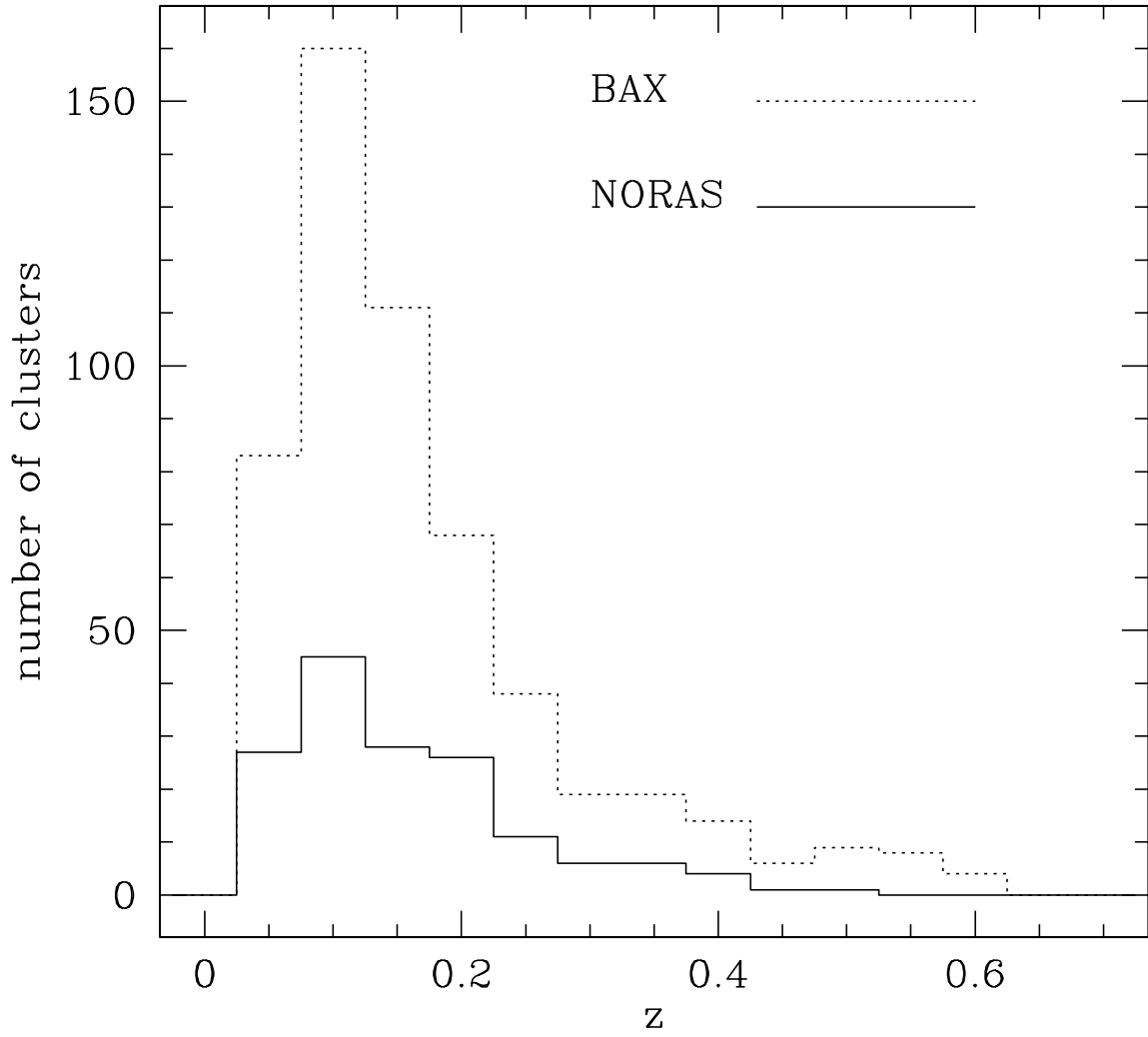


Fig. 24.— Redshift distribution of the matching clusters for BAX (dotted) and NORAS (solid)

Other attempts to cross-match optical cluster catalogs with X-ray selected ones yielded similar results. For instance, Koester et al. (2007) (see also Rykoff et al. 2008) limited their analysis to 99 clusters from NORAS and report that the fraction of clusters whose X-ray center disagrees with the optical center (chosen to be the BCG position) by more than $100 \text{ h}^{-1} \text{ kpc}$ is around 36%. Similar numbers and a distribution of the positional offset between optical and X-ray cluster centers that track ours can be found in Lopes et al. (2006).

The optical properties of matching clusters correlate well with the observed X-ray properties. In figs. 25 and 26 we show X ray luminosity and temperature versus richness for matching clusters. There is a clear trend in both luminosity and temperature. This is somewhat different from what found by Koester et al. (2007), who however only inspected 99 matches for NORAS/REFLEX on a smaller area and a smaller redshift range. Wen et al. (2009) look at X-ray correlations of their sample and find matching for about half the number of clusters matched with AMF.

The scalings shown in figs. 27 and 26 are well fitted with the functions and coefficients listed in Table 6. The scatter in both relations is quite substantial both in temperature and luminosity. (See Figures 25– 28.) Correlation coefficients do not show significant difference between all BAX and flux-limited samples.

As richness correlates very well with R_{200} estimates, the X-ray cluster properties also show good correlation with cluster radius. Table 6 gives the coefficients for the best fit lines for the X-ray measurement vs. optical parameter graphs. In the AMF catalog we also provide X-ray matching information.

6. Conclusions

We present a new optical catalog of 69,173 galaxy clusters extracted from the SDSS DR6. The catalog extends from $z=0.045$ to 0.78 on an area of $8,420 \text{ deg}^2$. The catalog was constructed using a maximum likelihood technique based on a matched filter approach which allows for the simultaneous determination of richness, core radius, redshift, with associated errors. The technique does not rely heavily on the presence of a luminous central red galaxy in order to detect a cluster, potentially allowing for the detection of clusters that do not present such a feature. In this paper, we also present the catalog of the three brightest galaxies associated with the clusters.

We find increasing number of clusters out to $z \simeq 0.45$, with a slope compatible with the expected number for a standard cosmology with $\sigma_8 \simeq 0.9$. Richness estimates correlate well with the radius of the clusters (R_{200}).

We provide a comparison with the existing maxBCG catalog on DR5 and $z \leq 0.3$ showing that the two catalogs only overlap at the 50% level over the whole range of redshifts. Matching between the two catalogs is high (80%–100%) for rich systems ($N_{gal}=100$ or $\Lambda_{200} > 100$) but is highly suppressed for smaller ones. Moreover, even where a match is found, the relation between

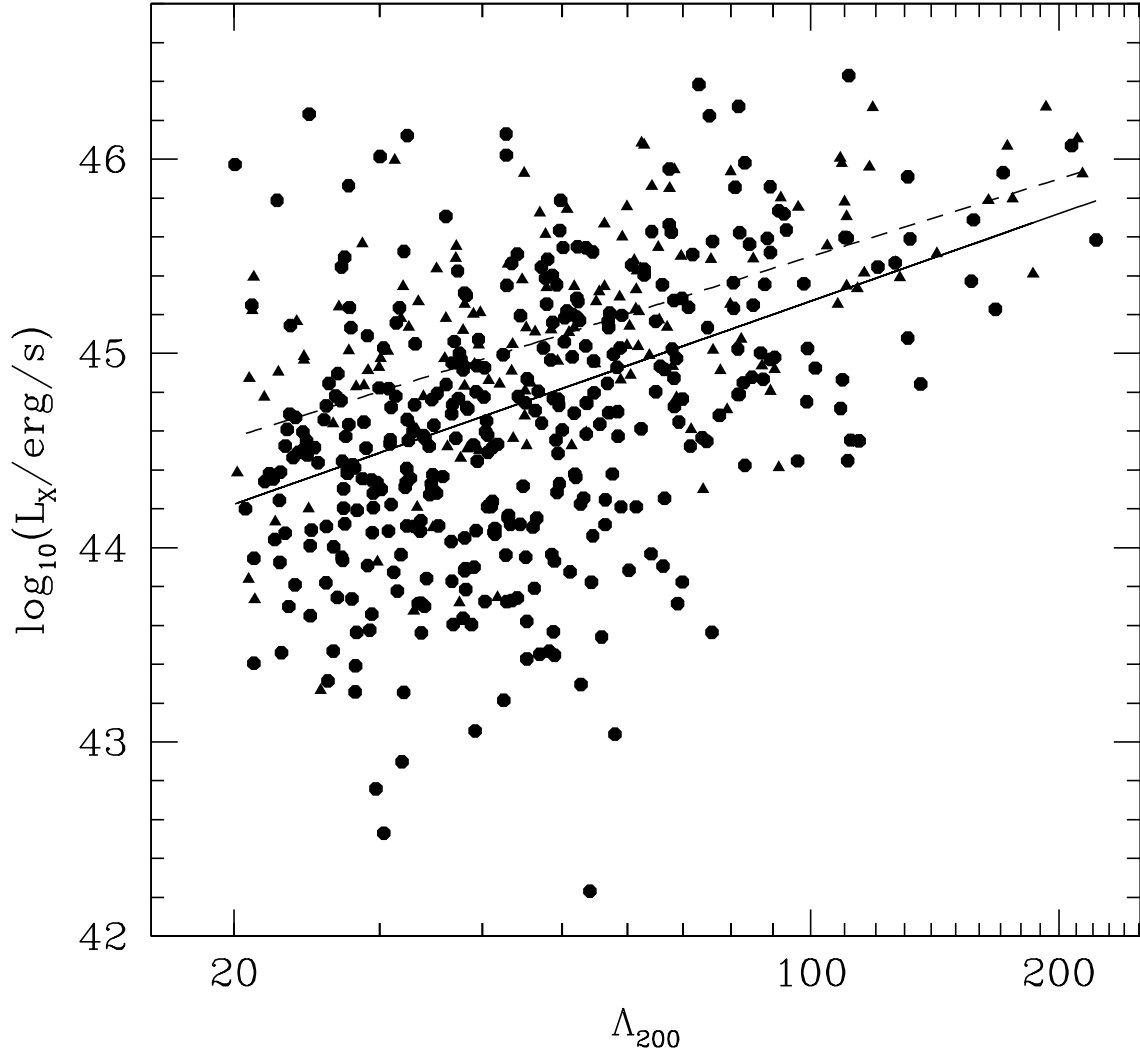


Fig. 25.— Luminosity of BAX clusters vs. richness of matched AMF clusters. L_X is measured in the 0.1-2.4 keV band. Triangles: NORAS clusters, circles: BAX. Solid line: fit to all data, dashed: NORAS.

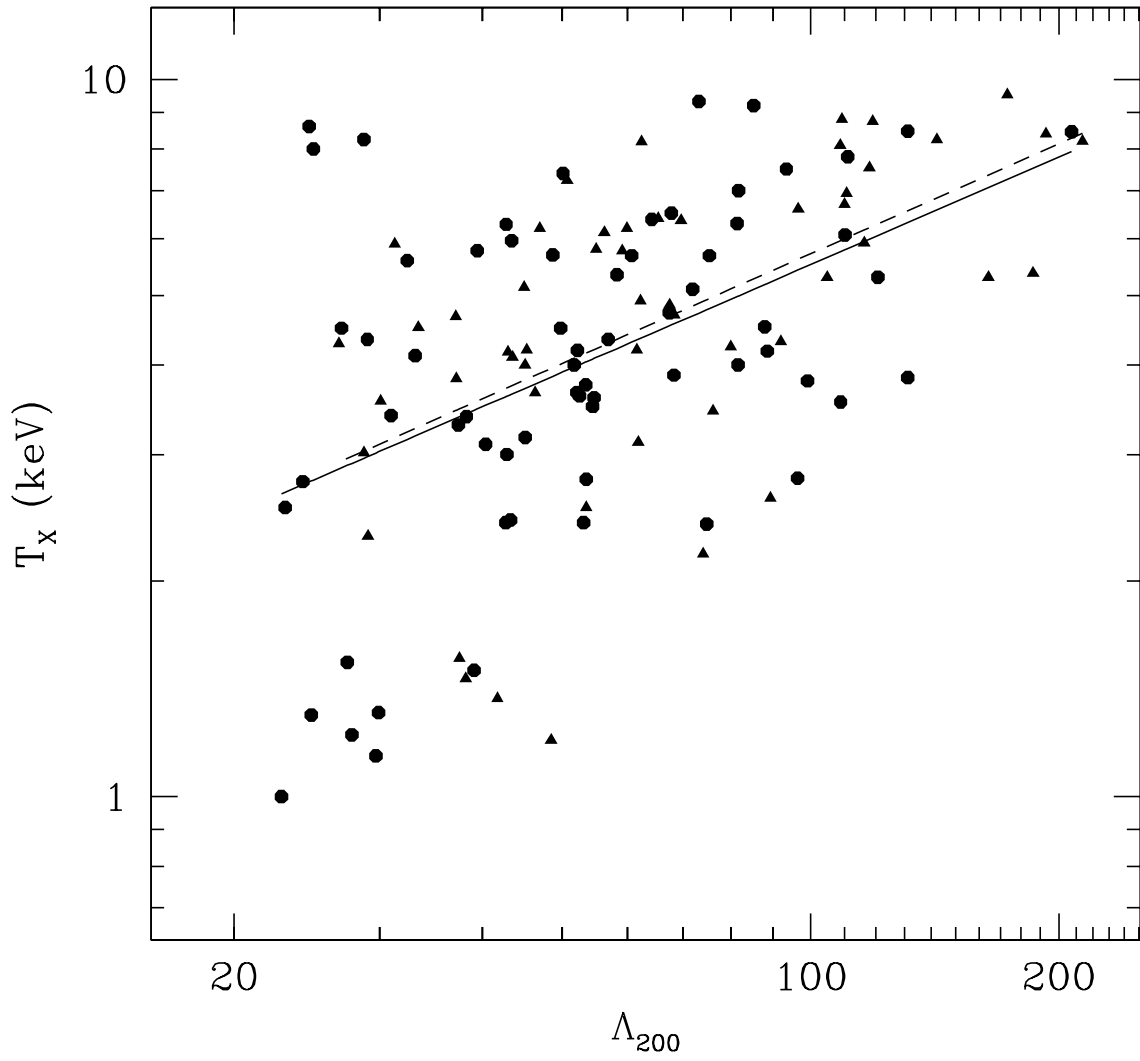


Fig. 26.— temperature of BAX clusters vs. richness of matched AMF clusters. Triangles: NORAS clusters, circles: BAX. Solid line: fit to all data, dashed: NORAS. .

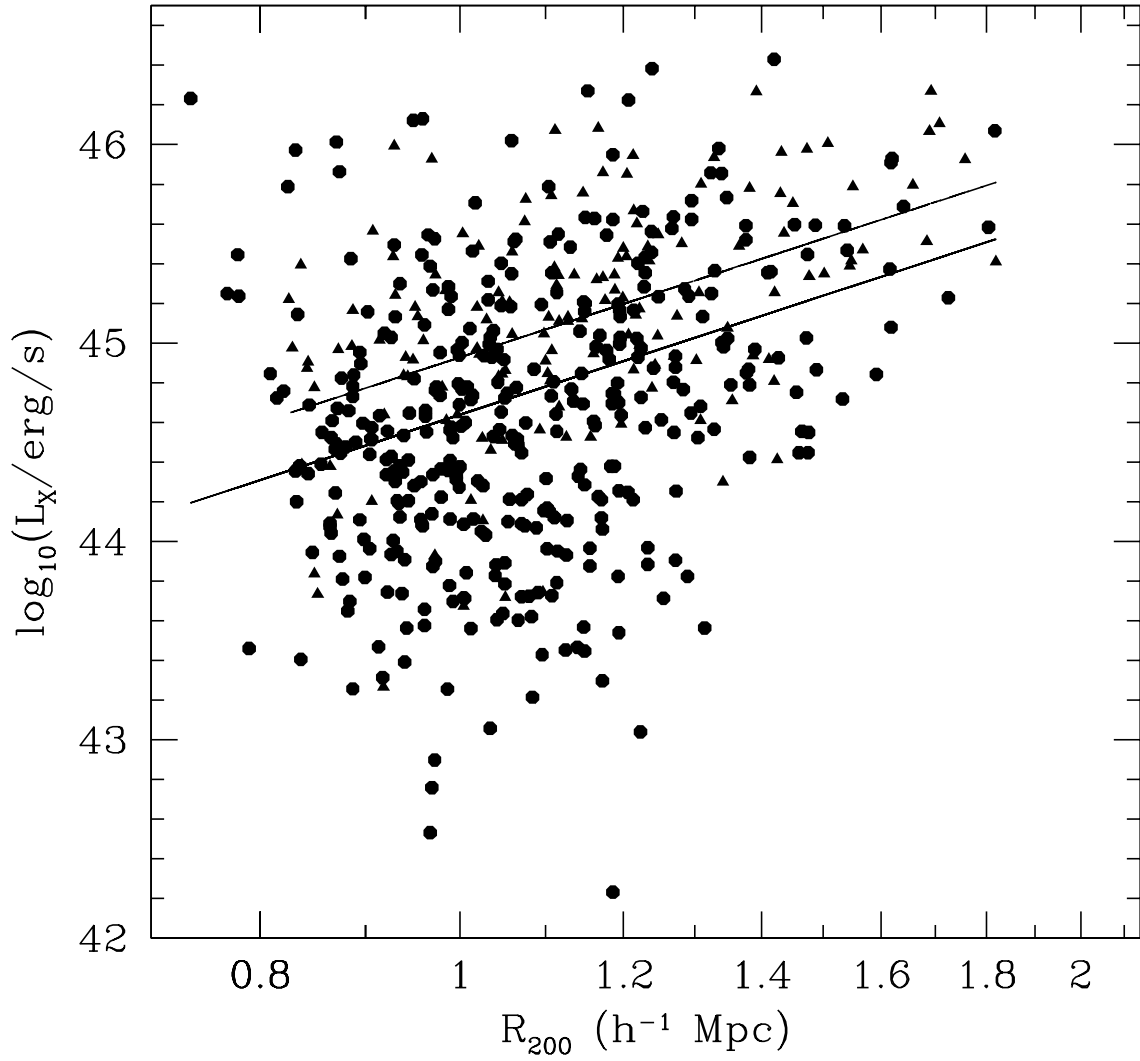


Fig. 27.— Luminosity of BAX clusters versus radius. Triangles: NORAS clusters, circles: BAX. Solid line: fit to all data, dashed: NORAS.

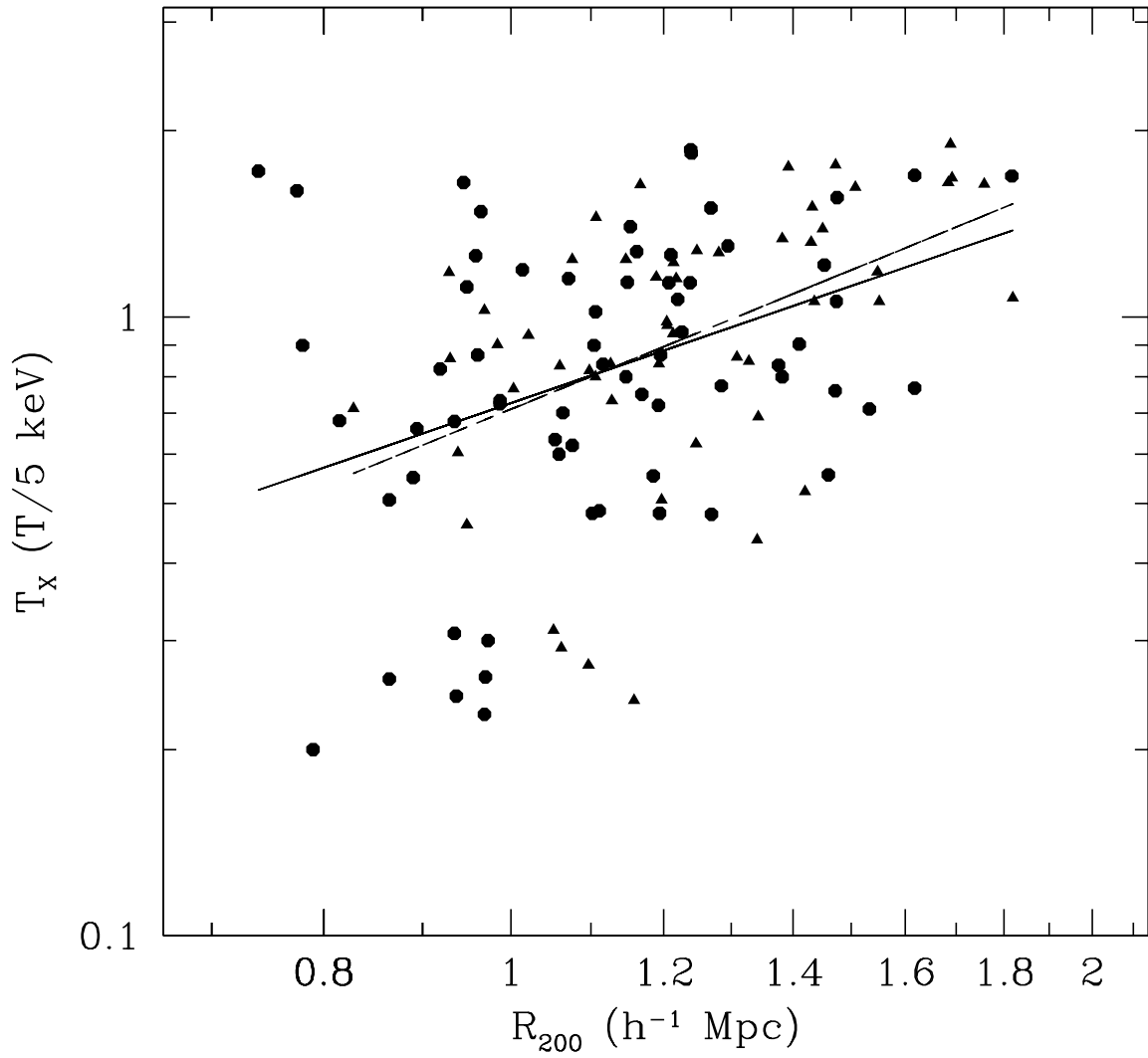


Fig. 28.— Temperature (in keV) of BAX clusters versus radius. Triangles: NORAS clusters, circles: BAX. Solid line: fit to all data, dashed: NORAS.

the two richness estimates is not very tight and the cluster centers determined by the methods can be far apart. Multiple reasons can generate these discrepancies, including, but not limited to, the definition of what a BCG is.

We compare our catalog with the WHL catalog which was also built with SDSS DR6 data. We find one-to-one matches for $> 70\%$ of WHL clusters with a richness, $R > 25$, however clusters from the AMF catalog with $\Lambda_{200} > 120$ match uniquely with $< 60\%$ of WHL clusters due to the tendency of the WHL finder method to fragment some richer AMF clusters. WHL clusters have one-to-one matches with AMF clusters at a rate of 55% for all redshifts, while 30% of AMF clusters have a unique WHL match when averaged over redshift.

When we compare the AMF and GMBCG catalogs in the overlapping regions, we find one-to-one matches for $> 60\%$ of AMF clusters with $\Lambda_{200} > 80$ and GMBCG clusters with $N_{gals} > 55$. The catalogs agree on the redshift of approximately 5,000 clusters to a margin of $|\Delta z| < 0.005$. The percentage of unique matches from each catalog is in the 30% to 40% for the overlapping portion of the redshift of the two catalogs ($0.10 \leq z \leq 0.55$). As is the case with both the maxBCG catalog and the WHL catalog, the GMBCG finder tends to split clusters that the AMF finder considers as one cluster.

We cross-match the new optical catalog with X-ray detected cluster samples, finding 539 matches, 155 of which with flux-limited X-ray samples (NORAS). We find good correlation between optical richness and both X-ray luminosity and temperature, with the same correlation found for flux limited and non flux-limited samples.

The present catalog is sufficiently broad and deep that it can be used for statistical studies of structure formation and for comparison with cluster finders in other wavelengths. In particular, we anticipate it can be used to assess redshift information for Sunyaev–Zel’dovich clusters detected by the Planck satellite in the Northern sky.

Further developments of this work will include the extension of the catalog to DR7 and inspection of areas of the sky with deep SDSS observations.

TS, AP and EP acknowledge support from NSF grant AST-0649899. EP is also supported by NASA grant NNX07AH59G and JPL–Planck subcontract 1290790, and would like to thank the Aspen Center for Physics for hospitality during the final stages of this work. This research has made use of: the SIMBAD database, operated at CDS, Strasbourg, France; the X-Rays Clusters Database (BAX), which is operated by the Laboratoire d’Astrophysique de Tarbes-Toulouse (LATT), under contract with the Centre National d’Etudes Spatiales (CNES); the NASA/IPAC Extragalactic Database (NED) which is operated by the Jet Propulsion Laboratory, California Institute of Technology, under contract with the National Aeronautics and Space Administration.

Funding for the Sloan Digital Sky Survey (SDSS) has been provided by the Alfred P. Sloan Foundation, the Participating Institutions, the National Aeronautics and Space Administration,

the National Science Foundation, the U.S. Department of Energy, the Japanese Monbukagakusho, and the Max Planck Society. The SDSS Web site is <http://www.sdss.org/>.

The SDSS is managed by the Astrophysical Research Consortium (ARC) for the Participating Institutions.

A. Photometric Flags for the SDSS Galaxy Sample

The following flags were set in our CAS Jobs queries to the SDSS database in order to ensure that our data sample had good photometry. The flags are given entirely in `TrueType` font, while the explanation for the flags being set are preceded by a bullet (\bullet) and follow each flag.

- ```
((case when (type_g=3) then 1 else 0 end) + (case when (type_r=3) then 1 else 0
end) + (case when (type_i=3) then 1 else 0 end)) > 1
```
- Object is of the type GALAXY;

```
and ((case when (dered_g < 11) then 1 else 0 end) + (case when (dered_r < 11) then
1 else 0 end) + (case when (dered_i < 11) then 1 else 0 end)) < 1
```

  - Apparent magnitude in the  $r$ -band, corrected for extinction, is  $> 11$ ;

```
and ((flags_r & 0x10000000)!=0)
```

  - Object detected in BINNED1;

```
and ((flags_r & 0x800a0)=0)
```

  - Eliminate objects with PEAKCENTER, NOPROFILE or NOTCHECKED set;

```
and (((flags_r & 0x400000000000)=0) or (psfmagerr_r<=0.2))
```

  - Eliminate objects where PSF\_FLU\_INTERP is not set or PSF magnitude error in the  $r$ -band is too small;

```
and ((flags_r & 0x58)!=0x8)
```

  - BLENDED, CHILD, and NODEBLEND objects have multiple peaks detected within them, and are candidates to be a deblending parent;

```
and ((flags_r & 0x40000=0) or (flags_r & 0x40000!=0 and flags_r & 0x800000000000=0))
```

  - The object cannot be saturated, or have its center too close to a saturated pixel;

```
and r<22
```

  - The apparent magnitude in the  $r$ -band is  $< 22$ .

### B. Retrieving the Catalog

The catalog (Table B.1), the error estimates for  $\Lambda_{200}$ ,  $r_c$ , and position for each cluster (Table B.2, the list of the three brightest galaxies per cluster (Table B.3), and the list of galaxies per cluster with  $\mathcal{L}_i(k) \geq 1.0$  (Table B.4) will be available upon request. Please e-mail one of the authors if you are interested in using them.

### C. Matching Clusters in Different Catalogs

The procedure for finding one-to-one matches between the AMF DR6 catalog and other cluster catalogs is as follows: i) using the centers of clusters in the AMF DR6 catalog as a basis, create a list of clusters from the other catalog whose centers lie within a given radius of the AMF DR6 cluster center, and whose redshifts are no more than 0.05 apart; ii) separate this list into two lists – one which takes all AMF clusters in the first list and pairs them with the cluster from the other catalog which is the smallest projected distance from its center, and one which takes every cluster listed from the other catalog and pairs it with the AMF cluster nearest its center; iii) if the same two clusters (AMF and other catalog) are paired in both lists from part ii, they are deemed a one-to-one match; iv) if the AMF cluster in the list is blended, the largest cluster on that site is selected for matching properties with the cluster in the other catalog. Other than the last step, the selection of one-to-one matches is based on position, and not on any other properties of the clusters involved.

As an example of a case where a match is rejected, AMF cluster 2292 matches with both Abell 1999 and Abell 2000, based on clusters with a center within  $R_{200}$  of AMF 2292. The angular separation is smaller for Abell 1999 than for Abell 2000. The match between AMF 2292 and Abell 2000 is deemed one-to-one, and the match with Abell 1999 is rejected.

### REFERENCES

- Abazajian, K. N., Adelman-McCarthy, J. K., Agüeros, M. A., et al. 2009, *ApJS*, 182, 543
- Adelman-McCarthy, J. K., Agüeros, M. A., Allam, S. S., et al. 2008, *ApJS*, 175, 297
- Adelman-McCarthy, J. K., Agüeros, M. A., Allam, S. S., et al. 2007, *ApJS*, 172, 634
- Abell, G. O. 1958, *ApJS*, 3, 211
- Allen, S. W., Rapetti, D. A., Schmidt, R. W., Ebeling, H., Morris, R. G., & Fabian, A. C. 2008, *MNRAS*, 383, 879
- Annis, J., Makler, M., Kent, S., et al. 2002, *BAAS*, 34, 778
- Bahcall, N. A. 1988, *ARA&A*, 26, 631
- Bahcall, N. A., Fan, X., & Cen, R. 1997, *ApJ*, 485, L53
- Baldry, I. K., Glazebrook, K., Budavári, T., et al. 2005, *MNRAS*, 358, 441
- Balestra, I., Tozzi, P., Ettori, S., et al. 2007, *A&A*, 462, 429
- Biviano, A. and Salucci, P. 2006, *A&A*, 452, 75

- Blain, A. W., Kneib, J.-P., Ivison, R. J., & Smail, I. 1999, *ApJ*, 512, L87
- Blanton, M. R., Hogg, D. W., Bahcall, N. A., et al. 2003, *ApJ*, 592, 819
- Böhringer, H., Voges, W., Huchra, J. P., et al. 2000, *ApJS*, 129, 435
- Böhringer, H., Schuecker, P., Guzzo, L., et al. 2004, *A&A*, 425, 367
- Butcher, H. & Oemler, Jr., A. 1978, *ApJ*, 219, 18
- Carlberg, R. G., Yee, H. K. C., Ellingson, E., Abraham, R., Gravel, P., Morris, S., & Pritchet, C. J. 1996, *ApJ*, 462, 32
- Cavagnolo, K. W., Donahue, M., Voit, G. M., & Sun, M. 2009, *ApJS*, 182, 12
- Csabai, I., Budavári, T., Connolly, A. J., et al. 2003, *AJ*, 125, 580
- Dahle, H. 2006, *ApJ*, 653, 954
- Diaferio, A., & Ostorero, L. 2009, *MNRAS*, 393, 215
- Dong, F., Pierpaoli, E., Gunn, J. E., & Wechsler, R. H. 2008, *ApJ*, 676, 868 (D08)
- Dressler, A. 1980, *ApJ*, 236, 351
- Garilli, B., Maccagni, D., & Andreon, S. 1999, *A&A*, 342, 408
- Girardi, M., Borgani, S., Giuricin, G., Mardirossian, F., and Mezzetti, M. 1998, *ApJ*, 506, 45
- Goto, T., Okamura, S., Yagi, M., et al. 2003a, *PASJ*, 54, 515
- Goto, T., Yamauchi, C., Fujita, Y., et al. 2003b, *MNRAS*, 346, 601
- Hansen, S. M., McKay, T. A., Wechsler, R. H., Annis, J., Sheldon, E. S., & Kimball, A. 2005, *ApJ*, 633, 122
- Hansen, Sarah M., Sheldon, Erin S., Wechsler, Risa H., & Koester, Benjamin P. 2009, *ApJ*, 699, 1333
- Hao, Jiangang, McKay, Timothy A., Koester, Benjamin P., et al. 2010, *ApJS*, 191, 254
- Ho, S., Lin, Y.-T., Spergel, D., & Hirata, C. 2009, *ApJ*, 697, 1358
- Ilbert, O., Tresse, L., Zucca, E., et al. 2005, *A&A*, 439, 863
- Jenkins, A., et al. 2001, *MNRAS*, 321, 372
- Katgert, P., Biviano, A., & Mazure, A. 2004, *ApJ*, 600, 657
- Kawasaki, W., Shimasaku, K., Doi, M., & Okamura, S. 1998, *A&AS*, 130, 567

- Kepner, J., Fan, X., Bachall, N., Gunn, J., Lupton, R., & Xu, G. 1999, *ApJ*, 517, 78
- Kim, R. S. J., Kepner, J. V., Postman, M., et al. 2002, *AJ*, 123, 20
- Koester, B. P., et. al. 2007, *ApJ*, 660, 239
- Lilly, S. J., Tresse, L., Hammer, F., Crampton, D., & Le Fevre, O. 1995, *ApJ*, 455, 108
- Lin, Y.-T. & Mohr, J. J. 2004, *ApJ*, 617, 879
- Lin, Y.-T., Mohr, J. J., & Stanford, S. A. 2004, *ApJ*, 610, 745
- Lin, Y.-T. & Mohr, J. J. 2007, *ApJS*, 170, 71
- Lopes, P. A. A., de Carvalho, R. R., Capelato, H. V., et al. 2006, *ApJ*, 648, 209
- Loveday, J., Peterson, B. A., Efstathiou, G., & Maddox, S. J. 1992, *ApJ*, 390, 338
- Loveday, J. 2004, *MNRAS*, 347, 601
- Maughan, B. J., Jones, C., Forman, W., & Van Speybroeck, L. 2008, *ApJS*, 174, 117
- Metcalfe, L., Kneib, J.-P., McBreen, B., et al. 2003, *A&A*, 407, 791
- Miller, C. J., Nichol, R. C., Reichart, D., et al. 2005, *AJ*, 130, 968
- Nagai, D. & Kravtsov, A. V. 2005, *ApJ*, 618, 557
- Nagamine, K., Fukugita, M., Cen, R., & Ostriker, J. P. 2001, *MNRAS*, 327, L10
- Navarro, J. F., Frenk, C. S., & White, S. D. M. 1997, *ApJ*, 490, 493
- Oyaizu, H., Marcos, L., Cunha, C. E., Lin, H., Frieman, J., & Sheldon, E. S. 2008, *ApJ*, 674, 768
- Pedersen, K. & Dahle, H. 2007, *ApJ*, 667, 26
- Pierpaoli, E., Scott, D., & White, M. 2001, *MNRAS*, 325, 77
- Pierpaoli, E., Borgani, S., Scott, D., & White, M. 2003, *MNRAS*, 342, 163
- Pipino, A. & Pierpaoli, E. 2010, *MNRAS*, 404, 1603
- Pipino, A., Szabo, T., Pierpaoli, E., & Dong, F. 2010, Arxiv e-prints, 1011.3017, submitted to *MNRAS* as a companion paper
- Planck Collaboration 2011, ArXiv e-prints, 1101.2401
- Popesso, P., Böhringer, H., Romaniello, M., & Voges, W. 2005, *A&A*, 433, 431
- Postman, M., Huchra, J. P., & Geller, M. J. 2003, *AJ*, 126, 1677

- Postman, M., Lubin, L. M., Gunn, J. E., Oke, J. B., Hoessel, J. G., Schneider, D. P., & Christensen, J. A. 1996, *AJ*, 111, 615
- Rapetti, D., Allen, S. W., & Mantz, A. 2008, *MNRAS*, 388, 1265
- Reiprich, T. H. & Böhringer, H. 2002, *ApJ*, 567, 716
- Rines, K., Diaferio, A., & Natarajan, P. 2007, *ApJ*, 657, 183
- Rozo, E., Wechsler, R. H., Rykoff, E. S., et al. 2009, *ArXiv e-prints*, 3702
- Rykoff, E. S., McKay, T. A., Becker, M. R., et al. 2008, *ApJ*, 675, 1106
- Santos, M. R., Ellis, R. S., Kneib, J.-P., Richard, J., & Kuijken, K. 2004, *ApJ*, 606, 683
- Schechter, P. 1976, *ApJ*, 203, 297
- Seljak, U. 2002, *MNRAS*, 337, 769
- Smail, I., Ivison, R. J., Blain, A. W., & Kneib, J.-P. 2002, *MNRAS*, 331, 495
- Staniszewski, Z., Ade, P. A. R., Aird, K. A., et al. 2009, *ApJ*, 701, 32
- Wang, S., Haiman, Z., Hu, W., Khoury, J., & May, M. 2005, *Phys. Rev. Lett.*, 95, 011302
- Wen, Z. L., Han, J. L., & Liu, F. S. 2009, *ApJS*, 183, 197
- White, M., & Kochanek, C. S. 2002, *ApJ*, 574, 24
- York, D. G., Adelman, J., Anderson, Jr., J. E., et al. 2000, *AJ*, 120, 1579
- Zheng, Z., et al. 2005, *ApJ*, 633, 791

Table 6. X-ray Comparison Fitting Coefficients

|                    | All BAX matches     |       | NORAS matches       |       |
|--------------------|---------------------|-------|---------------------|-------|
|                    | $L_X$               | $T_X$ | $L_X$               | $T_X$ |
|                    | erg s <sup>-1</sup> | keV   | erg s <sup>-1</sup> | keV   |
| $\Lambda_{200}, A$ | 42.28               | -0.25 | 42.84               | -0.26 |
| $\Lambda_{200}, B$ | 1.49                | 0.498 | 1.33                | 0.508 |
| $R_{200}, A$       | 44.64               | -0.14 | 44.93               | -0.15 |
| $R_{200}, B$       | 3.40                | 1.08  | 3.40                | 1.28  |

Note. — Fits to the data are of the form  $\log_{10}(X) = A + B \log_{10}(Y)$ , where X is the X-ray observable and Y is the optical observable.  $R_{200}$  values are always in terms of  $1 \text{ h}^{-1} \text{ Mpc}$ . For fits of  $T_X$  vs.  $R_{200}$ , the X-ray value that is fit is  $T_X/5 \text{ keV}$ .

Table B.1. Cluster Catalog

| a.b.d.f | RA<br>(degrees) | DEC     | z      | $\Delta \ln \mathcal{L}$ | $\Lambda_{200}$<br>( $L^*$ ) | $R_{200}$<br>( $h^{-1}$ Mpc) | ... | RA        | DEC<br>of maxBCG match | z        | WHL<br>match     | BAX<br>match |
|---------|-----------------|---------|--------|--------------------------|------------------------------|------------------------------|-----|-----------|------------------------|----------|------------------|--------------|
| 1.0.0.1 | 140.1428        | 30.4833 | 0.3763 | 307.9678                 | 270.1469                     | 1.864                        | ... | -         | -                      | -        | -                | -            |
| 2.0.0.2 | 139.4840        | 51.7226 | 0.2845 | 238.2846                 | 253.6087                     | 1.890                        | ... | -         | -                      | -        | -                | -            |
| 3.0.0.3 | 340.8307        | -9.5867 | 0.4778 | 196.6117                 | 225.8704                     | 1.686                        | ... | -         | -                      | -        | J224319.8-093530 | -            |
| 4.0.0.0 | 174.0642        | 40.0617 | 0.3627 | 226.7762                 | 224.6193                     | 1.760                        | ... | -         | -                      | -        | J113615.9+400432 | -            |
| 5.0.0.5 | 188.5358        | 15.2114 | 0.2851 | 248.5700                 | 222.0067                     | 1.804                        | ... | 188.47087 | 15.194643              | 0.275450 | J123416.3+151326 | Abell 1560   |

Note. — In the first column, a is the rank of the cluster in richness; b=1 if the cluster is on the edge of a stripe, b=0, otherwise; d=1 if a cluster has at least five galaxies with spectroscopic measurements as members, d=0 otherwise; f=a if a cluster is unique to a site, f=0 if the cluster is the richest member on a blended site, f equals a of the richest cluster on a site if the cluster in question is of lower richness, and f=999999 if the cluster contains no galaxies with  $\mathcal{L} \geq 1$ .



Table B.2. Error Ranges for  $\Lambda_{200}$ ,  $r_c$ , and Position of AMF DR6 Clusters

| Cluster Rank | Ranges for $\Lambda_{200}$ |          |          |          | Ranges for $r_c$ ( $h^{-1}$ Mpc) |     |        | Ranges for RA (degrees) |     |          | Ranges for DEC (degrees) |     |         |
|--------------|----------------------------|----------|----------|----------|----------------------------------|-----|--------|-------------------------|-----|----------|--------------------------|-----|---------|
|              | 95%(-)                     | 68%(-)   | 68%(+)   | 95%(+)   | 95%(-)                           | ... | 95%(+) | 95%(-)                  | ... | 95%(+)   | 95%(-)                   | ... | 95%(+)  |
| 1            | 215.7585                   | 238.7345 | 314.8423 | 342.1262 | 0.856                            | ... | 1.040  | 140.1395                | ... | 140.1760 | 30.4627                  | ... | 30.4873 |
| 2            | 158.0631                   | 179.6325 | 259.1696 | 286.1313 | 0.092                            | ... | 0.333  | 139.4740                | ... | 139.5033 | 51.7149                  | ... | 51.7326 |
| 3            | 143.1763                   | 162.3866 | 229.6224 | 254.8358 | 0.379                            | ... | 0.619  | 340.8284                | ... | 340.8500 | -9.6010                  | ... | -9.5755 |
| 4            | 155.5172                   | 175.8150 | 243.8724 | 267.7522 | 0.432                            | ... | 1.079  | 174.0449                | ... | 174.0700 | 40.0459                  | ... | 40.0702 |
| 5            | 158.4287                   | 179.6705 | 250.4767 | 276.4389 | 0.515                            | ... | 0.721  | 188.5200                | ... | 188.5551 | 15.1964                  | ... | 15.2299 |

Note. — For our error estimates, we assume the shape of the likelihood surface to be Gaussian. We find the extrema of the 68% and 95% confidence ranges when varying any two of richness, core radius, and position. These extrema are reported for both the 68% and 95% confidence ranges for the four quantities listed in the table above.

Table B.3. Three Brightest BCG Candidates of AMF DR6 Clusters

| a.b | SDSS ID            | RA       | DEC     | $k_{z=0.0}$ | $k_{z=0.3}$ | $k_{z=0.5}$ | $m^u$    | ... | $\sigma_{mz}$ | $z_{photo}$ | $z_{spec}$ | $\Lambda_{200}$ | $M^r$     |
|-----|--------------------|----------|---------|-------------|-------------|-------------|----------|-----|---------------|-------------|------------|-----------------|-----------|
| 1.1 | 587738947204284630 | 140.1074 | 30.4941 | -0.39217    | 0.20848     | 0.35816     | 19.21763 | ... | 0.01958       | 0.47638     | 1.00000    | 270.1469        | -24.39410 |
| 1.2 | 588017978339819919 | 140.2203 | 30.4797 | -0.39447    | 0.18756     | 0.32479     | 21.55961 | ... | 0.03421       | 0.32691     | 1.00000    | 270.1469        | -22.97133 |
| 1.3 | 588017978339819858 | 140.2966 | 30.4625 | -0.39447    | 0.20583     | 0.35874     | 22.12220 | ... | 0.02739       | 0.33160     | 1.00000    | 270.1469        | -22.45713 |
| 2.1 | 587729388215337136 | 139.4726 | 51.7270 | -0.37158    | 0.13973     | 0.27418     | 21.04132 | ... | 0.01091       | 0.22093     | 1.00000    | 253.6087        | -23.80616 |
| 2.2 | 587729388215337173 | 139.5155 | 51.7261 | -0.34441    | 0.09874     | 0.18445     | 21.25870 | ... | 0.01742       | 0.22468     | 1.00000    | 253.6087        | -22.25050 |
| 2.3 | 587729388215337224 | 139.5786 | 51.7295 | -0.33982    | 0.10316     | 0.08794     | 21.64812 | ... | 0.02285       | 0.24272     | 1.00000    | 253.6087        | -22.16702 |

Note. — In the description above, a is the cluster rank in richness, and b is the rank of the galaxy in brightness in the  $r$ -band for cluster members. The complete table has apparent magnitudes and their errors in all five bands. The absolute magnitude in the  $r$ -band,  $M^r$ , is computed at the redshift of the cluster using the interpolated value of the  $k$ -correction. If there is no  $z_{photo}$ , the column is set to -1.0; for no  $z_{spec}$ , the column is set to 1.0.

Table B.4. Galaxy Membership as Determined by Likelihood Difference

| rank | SDSS ID            | RA       | DEC     | $k_{z=0.0}$ | $k_{z=0.3}$ | $k_{z=0.5}$ | $m^u$    | ... | $\sigma_{mz}$ | $z_{photo}$ | $err(z_p)$ | $z_{spec}$ | $err(z_s)$ | $\mathcal{L}_i(k)$ |
|------|--------------------|----------|---------|-------------|-------------|-------------|----------|-----|---------------|-------------|------------|------------|------------|--------------------|
| 1    | 587738947204219607 | 139.9842 | 30.4446 | -0.32752    | 0.12719     | 0.24940     | 22.66395 | ... | 0.09668       | 0.33350     | 0.10170    | 1.00000    | 1.0000000  | 1.016546           |
| 1    | 587738947204219643 | 139.9797 | 30.4800 | -0.38423    | 0.17791     | 0.29166     | 22.70960 | ... | 0.09613       | 0.39693     | 0.07813    | 1.00000    | 1.0000000  | 1.081769           |
| 1    | 587738947204219662 | 139.9861 | 30.4828 | -0.38392    | 0.17251     | 0.29184     | 22.68239 | ... | 0.09734       | 0.42199     | 0.06025    | 1.00000    | 1.0000000  | 1.206062           |
| 1    | 587738947204284458 | 140.0525 | 30.5400 | -0.39447    | 0.18599     | 0.27622     | 22.91521 | ... | 0.07725       | 0.34760     | 0.05497    | 1.00000    | 1.0000000  | 1.817760           |
| 1    | 587738947204284490 | 140.1159 | 30.5296 | -0.34927    | 0.14850     | 0.11052     | 23.57531 | ... | 0.11600       | 0.30946     | 0.07936    | 1.00000    | 1.0000000  | 2.263241           |

Note. — Galaxies which have no spectroscopic redshift (or spectroscopic redshift error) are assigned a value of 1.0 for that column. Galaxies with no photometric redshift estimate (or error) appear with a value of -1.0. The full table has apparent magnitudes and their errors for all five bands.